6.8 Hz, 2H, CO–CH_2–CH_2–CH_2–CO), 2.18 (dd, J = 6.8, 6.8 Hz, 2H, CO–CH_2–CH_2–CH_2–CO), 1.98 (q, J = 7.6 Hz, 2H, –CH_2–CH_3), 1.84 (dd, J = 6.8, 6.8 Hz, 2H, CO–CH_2–CH_2–CH_2–CO), 0.78 (t, J = 7.6 Hz, 3H, –CH_2–CH_3). Anal. Calcd for $C_{85}H_{89}N_6O_{25}P$: C, 62.80; H, 5.52; N, 5.17%. Found: C, 62.78; H, 5.51; N, 5.29%.

3-*O*-Acylated Compounds 45a and 45b. 45a: To a solution of **29** (434 mg, 267 μmol) and (*R*)-3-(4-trifluoromethylbenzyloxy)-decanoic acid (**20**) (150 mg, 433 μmol) in anhydrous CH_2Cl_2 (10 mL) were added DMAP (3.3 mg, 27 μmol) and DIC (125 μL, 798 μmol) at room temperature under Ar atmosphere and the mixture was stirred for 2 h. To the reaction mixture was added toluene (10 mL) and the mixture was subjected to affinity separation (13 g × 3). After untagged compounds were eluted with toluene–CH_2Cl_2 (1:1) and CH_2Cl_2, **45a** was obtained as a pale yellow solid (435 mg, 84%) by elution with CH_2Cl_2–MeOH (1:1) and evaporation of the solvents. $[\alpha]_D^{23}$ = +22.9 (*c* 0.94, $CHCl_3$). ESI-MS (positive) m/z 1975.42 $[M + Na]^+$, 999.35 $[M + 2Na]^{2+}$. ^{1}H NMR (400 MHz, DMSO-d_6, 40 °C): δ 7.84 (d, J = 7.2 Hz, 2H, $(C_6H_4)_2$–CH–CH_2–OCO–), 7.67 (dd, J = 8.9, 7.2 Hz, 2H, $(C_6H_4)_2$–CH–CH_2–OCO–), 7.63 (dd, J = 7.3, 6.9 Hz, 2H, –OCH_2–$COOCH_2$–C_6H_5), 7.55 (d, J = 8.0 Hz, 2H, p-CF_3–C_6H_4–CH_2–), 7.52 (dd, J = 7.2, 7.2 Hz, 2H, $(C_6H_4)_2$–CH–CH_2–OCO–), 7.41–7.31 (m, 12H, $(C_6H_4)_2$–CH–CH_2–OCO–, p-RCONH–C_6H_4–CH_2–, p-CF_3–C_6H_4–CH_2–, and C_6H_5–CH_2–), 7.30–7.25 (m, 6H, BA–CH_2–C_6H_4–CH_2NHCO–, o-C_6H_4-$(CH_2O)_2$P–, and –OCH_2–$COOCH_2$–C_6H_5), 7.15–7.10 (m, 4H, o-$C_6H_4(CH_2O)_2$P– and BA–CH_2–C_6H_4–CH_2NHCO–), 6.95 (d, J = 8.0 Hz, 2H, p-RCONH–C_6H_4–CH_2–), 5.95–5.83 (m, 1H, –OCH_2–CH=CH_2 of Alloc), 5.43 (d, J = 6.5 Hz, 1H, NH), 5.28 (d, J = 15.4 Hz, 1H, –OCH_2–CH=CH_2 of Alloc), 5.21 (d, J = 10.5 Hz, 1H, –OCH_2–CH=CH_2 of Alloc), 5.17–5.07 (m, 9H, NH, H-3, H-3′, o-$C_6H_4(CH_2O)_2$P, and –OCH_2–$COOCH_2$–C_6H_5), 4.95 (brs, 1H, H-1), 4.79 (dd, J = 10.3, 10.3 Hz, 2H, p-RCONH–C_6H_4–CH_2–), 4.67 (d, J = 2.8 Hz, 1H, –OCH_2–C≡CH of Proc), 4.61–4.52 (m, 8H, H-1′, H-4′, C_6H_5–CH_2–, p-CF_3–C_6H_4–CH_2–, –OCH_2–C≡CH of Proc, and –OCH_2–CH=CH_2 of Alloc), 4.48 (d, J = 12.5 Hz, 1H, C_6H_5–CH_2–), 4.39 (d, J = 7.2 Hz, 2H, $(C_6H_4)_2$–CH–CH_2–OCO–), 4.21 (dd, J = 7.2, 7.2 Hz, 1H, $(C_6H_4)_2$–CH–CH_2–OCO–), 4.18–4.10 (m, 4H, –OCH_2–$COOCH_2$–C_6H_5 and BA–CH_2–C_6H_4–CH_2NHCO–), 3.93–3.86 (m, 2H, H-2 and H-6′a), 3.78 (brs, 1H, β-CH of 3-*O*-acyl), 3.76–3.72 (m, 3H, H-4, H-6a, and H-5′), 3.65–3.58 (m, 4H, H-5, H-6b, H-2′, and H-6′b), 3.07 (s, 2H, BA–CH_2–C_6H_4–CH_2NHCO–), 2.51–2.45 (m, 3H, –OCH_2–C≡CH of Proc and α-CH_2 of 3-*O*-acyl), 2.29 (dd, J = 6.8, 6.8 Hz, 2H, –CO–CH_2–CH_2–CH_2–CO–), 2.18 (dd, J = 6.8, 6.8 Hz, 2H, –CO–CH_2–CH_2–CH_2–CO–), 1.96 (q, J = 7.6 Hz, 2H, –CH_2–CH_3 of BA), 1.81 (dd, J = 6.8; 6.8 Hz, 2H, –CO–CH_2–CH_2–CH_2–CO–), 1.60–1.47 (m, 2H, γ-CH_2 of 3-*O*-acyl), 1.31–0.99 (m, 10H, CH_2 × 5), 0.79 (t, J = 7.6 Hz, 3H, –CH_2–CH_3 of 3-*O*-acyl), 0.74 (t, J = 7.2 Hz, 3H, –CH_2–CH_3 of BA).

45b: In a manner similar to the synthesis of **45a**, **29** (221 mg, 136 μmol) was acylated with (*R*)-3-(dodecanoyloxy)decanoic acid (**21**) to yield **45b** as a pale yellow solid (247 mg, 93%). ESI-MS (positive) m/z 1977.87 $[M + H]^+$, 1999.81 $[M + Na]^+$, 1000.41 $[M + H + Na]^{2+}$.

3-,3′-*O*-Diacylated Compounds 46a, 46b, 46c, and 46d. 46a: To a degassed solution of **45a** (140 mg, 71.6 μmol) in anhydrous THF (4.0 mL) was added (1,5-cyclooctadiene)[bis(methyldiphenylphosphine)]iridium(I) hexafluorophosphate (65.0 mg, 76.9 μmol). After activation of the iridium catalyst with hydrogen three times (each 30 s), the mixture was stirred under Ar atmosphere at room temperature for 1.5 h. The mixture was concentrated in vacuo to give crude 3′-*O*-deprotected product. To a solution of the crude 3′-*O*-free product and (*R*)-3-(4-trifluoromethylbenzyloxy)decanoic acid (**20**) (50.0 mg, 144 μmol) in anhydrous CH_2Cl_2 (4.0 mL) were added DIC (40.0 μL, 255 μmol) and DMAP (1.0 mg, 8.2 μmol) at room temperature under Ar atmosphere. After stirring for 8 h, the reaction mixture was directly subjected to affinity separation (13 g × 1) to give **46a** as a pale yellow solid (117 mg, 75%). $[\alpha]_D^{24}$ = +18.3 (*c* 0.67, $CHCl_3$). ESI-MS (positive) m/z 2222.34 $[M + Na]^+$. ^{1}H NMR (400 MHz, DMSO-d_6, 40 °C): δ 9.79 (s, 1H, NH), 8.22 (t, J = 3.8 Hz, 2H, NH), 7.84 (d, J = 7.6 Hz, 2H, $(C_6H_4)_2$–CH–CH_2–OCO–), 7.66 (dd, J = 7.3, 6.9 Hz, 2H, –OCH_2–$COOCH_2$–C_6H_5), 7.58 (dd, J = 8.1, 7.6 Hz, 2H, $(C_6H_4)_2$–CH–CH_2–OCO–), 7.54 (d, J = 8.0 Hz, 4H, p-CF_3–C_6H_4–CH_2–), 7.52 (d, J = 8.1 Hz, 2H, $(C_6H_4)_2$–CH–CH_2–OCO–), 7.41–7.31 (m, 14H, $(C_6H_4)_2$–CH–CH_2–OCO–, p-RCONH–C_6H_4–CH_2–, p-CF_3–C_6H_4–CH_2–, and C_6H_5–CH_2–), 7.30–7.25 (m, 6H, BA–CH_2–C_6H_4–CH_2NHCO–, o-C_6H_4-$(CH_2O)_2$P–, and –OCH_2–$COOCH_2$–C_6H_5), 7.14–7.10 (m, 4H, o-$C_6H_4(CH_2O)_2$P– and BA–CH_2–C_6H_4–CH_2NHCO–), 6.95 (d, J = 8.1 Hz, 2H, p-RCONH–C_6H_4–CH_2–), 5.95–5.85 (m, 1H, –OCH_2–CH=CH_2 of Alloc), 5.44 (d, J = 6.5 Hz, 1H, NH), 5.38 (dd, J = 10.1, 10.1 Hz, 1H, H-3′), 5.31 (d, J = 14.5 Hz, 1H, –OCH_2–CH=CH_2 of Alloc), 5.23 (d, J = 10.5 Hz, 1H, –OCH_2–CH=CH_2 of Alloc), 5.18–5.08 (m, 8H, NH, H-3, o-$C_6H_4(CH_2O)_2$P, and –OCH_2–$COOCH_2$–C_6H_5), 4.95 (brs, 1H, H-1), 4.60 (dd, J = 10.1, 10.1 Hz, 2H, p-RCONH–C_6H_4–CH_2–), 4.53–4.47 (m, 9H, H-1′, H-4′, C_6H_5–CH_2–, p-CF_3–C_6H_4–CH_2–, and –OCH_2–CH=CH_2 of Alloc), 4.39 (d, J = 7.2 Hz, 2H, $(C_6H_4)_2$–CH–CH_2–OCO–), 4.21 (dd, J = 7.2, 7.2 Hz, 1H, $(C_6H_4)_2$–CH–CH_2–OCO–), 4.15–4.07 (m, 4H, –OCH_2–$COOCH_2$–C_6H_5 and BA–CH_2–C_6H_4–CH_2NHCO–), 3.95–3.87 (m, 2H, H-2 and H-6′a), 3.81–3.74 (m, 4H, H-4, H-6a, H-5′, and β-CH of 3-*O*-acyl), 3.68–3.58 (m, 5H, H-5, H-6b, H-2′, H-6′b, and β-CH of 3′-*O*-acyl), 3.06 (d, J = 3.7 Hz, 2H, BA–CH_2–C_6H_4–CH_2NHCO–), 2.65 (dd, J = 15.0, 5.3 Hz, 1H, α-CH_2 of 3-*O*-acyl), 2.53–2.45 (m, 2H, α-CH_2 of 3-*O*-acyl and 3′-*O*-acyl), 2.41 (dd, J = 15.1, 5.6 Hz, 1H, α-CH_2 of 3′-*O*-acyl), 2.28 (dd, J = 7.1, 7.1 Hz, 2H, –CO–CH_2–CH_2–CH_2–CO–), 2.17 (dd, J = 7.1, 7.1 Hz, 2H, –CO–CH_2–CH_2–CH_2–CO–), 1.96 (q, J = 7.3 Hz, 2H, –CH_2–CH_3 of BA), 1.81 (dd, J = 7.1, 7.1 Hz, 2H, –CO–CH_2–CH_2–CH_2–CO–), 1.55–1.48 (m, 4H, γ-CH_2 of 3-*O*-acyl and 3′-*O*-acyl), 1.31–0.99 (m, 20H, CH_2 × 10), 0.86–0.79 (m, 6H, –CH_2–CH_3 of 3-*O*-acyl and 3′-*O*-acyl), 0.75 (t, J = 7.1 Hz, 3H, –CH_2–CH_3 of BA).

46b: In a manner similar to the synthesis of **46a**, **45a** (288 mg, 147 μmol) was deprotected and acylated with (*R*)-3-(dodecanoyloxy)decanoic acid (**21**) to yield **46b** as a pale yellow solid (252 mg, 77%). ESI-MS (positive) m/z 2249.29 $[M + Na]^+$.

46c: To a solution of **45b** (235 mg, 119 μmol) in AcOH (5.0 mL) was added Zn–Cu couple (200 mg) at room temperature, and the mixture was stirred for 2 h. After insoluble materials were filtered off, the filtrate was concentrated in vacuo, and the residual AcOH was removed by co-evaporation with toluene three times. The residue was dissolved in EtOAc, washed successively with saturated aqueous $NaHCO_3$ and brine, dried over $MgSO_4$, and concentrated in vacuo. To a solution of the residue and (*R*)-3-(dodecanoyloxy)decanoic acid (**21**) (120 mg, 346 μmol) in anhydrous CH_2Cl_2 (5.0 mL) were added DMAP (1.5 mg, 12 μmol) and DIC (110 μL, 703 μmol) at room temperature under Ar atmosphere and the mixture was stirred for 11 h. To the reaction mixture

was added toluene (5.0 mL) and the mixture was subjected to affinity separation (13.0 g × 3) to give **46c** as a pale yellow solid (155 mg, 59%). ESI-MS (positive) m/z 2224.80 $[M+H]^+$, 2246.33 $[M+Na]^+$, 1123.62 $[M+H+Na]^{2+}$, 1134.97 $[M+2Na]^{2+}$.

46d: In a manner similar to the synthesis of **46c**, **45b** (98.2 mg, 49.6 μmol) was deprotected and acylated with (*R*)-3-(4-trifluoromethylbenzyloxy)decanoic acid (**20**) to yield **46d** as a pale yellow solid (59.6 mg, 59%). ESI-MS (positive) m/z 2270.29 $[M+Na]^+$, 1136.00 $[M+H+Na]^{2+}$.

2′-N-,3-,3′-O-Triacylated Compounds 47a, 47b, 47c, 47d, 47e, and 47f. 47a: To a solution of **46a** (50.0 mg, 22.7 μmol) in anhydrous THF (2.0 mL) was added Et_3N (31.7 μL, 226 μmol), HCO_2H (8.6 μL, 220 μmol), and tetrakis(triphenylphosphine)-palladium(0) (5.2 mg, 4.5 μmol) at room temperature under Ar atmosphere. After the mixture was stirred for 1 h, EtOAc was added. The organic layer was washed with 1 M HCl, saturated aqueous $NaHCO_3$, and brine. The EtOAc layer was dried over $MgSO_4$ and concentrated in vacuo to give 2′-N-deprotected product. To a solution of the crude 2-N-free product and (*R*)-3-(dodecanoyloxy)decanoic acid (**21**) (42.1 mg, 114 μmol) in anhydrous CH_2Cl_2 (4.0 mL) were added DIC (36.0 μL, 230 μmol) at room temperature under Ar atmosphere. After stirring for 18 h, toluene (4.0 mL) was added and the reaction mixture was subjected to affinity separation (13 g × 1) to give **47a** as a pale yellow solid (38.1 mg, 70%). ESI-MS (positive) m/z 2268.61 $[M+H]^+$, 2490.30 $[M+Na]^+$, 1245.33 $[M+2Na]^{2+}$. ^{1}H NMR (400 MHz, DMSO-d_6, 40 °C): δ 8.22 (s, 1H, NH), 7.83 (d, J = 7.3 Hz, 2H, $(C_6H_4)_2$–CH–CH_2–OCO–), 7.65 (dd, J = 8.3, 7.3 Hz, 2H, –OCH_2–$COOCH_2$–C_6H_5), 7.56 (dd, J = 8.3, 7.3 Hz, 2H, $(C_6H_4)_2$–CH–CH_2–OCO–), 7.50 (d, J = 7.3 Hz, 4H, p-CF_3–C_6H_4–CH_2–), 7.39 (dd, J = 7.3, 7.3 Hz, 2H, $(C_6H_4)_2$–CH–CH_2–OCO–), 7.35–7.30 (m, 14H, $(C_6H_4)_2$–CH–CH_2–OCO–, p-RCONH–C_6H_4–CH_2–, p-CF_3–C_6H_4–CH_2–, and C_6H_5–CH_2–), 7.28–7.25 (m, 6H, BA–CH_2–C_6H_4–CH_2NHCO–, o-C_6H_4-$(CH_2O)_2$P–, and –OCH_2–$COOCH_2$–C_6H_5), 7.21 (dd, J = 8.2, 4.8 Hz, 2H, o-$C_6H_4(CH_2O)_2$P), 7.14 (d, J = 7.8 Hz, 2H, BA–CH_2–C_6H_4–CH_2NHCO–), 7.08 (d, J = 7.8 Hz, 2H, p-RCONH–C_6H_4–CH_2–), 6.57 (d, J = 8.8 Hz, 1H, 2′-NH), 6.11 (d, J = 8.5 Hz, 1H, 2-NH), 5.45 (d, J = 6.5 Hz, 1H, NH), 5.45 (dd, J = 10.2, 10.2 Hz, 1H, H-3′), 5.33 (dd, J = 10.5, 10.5 Hz, 1H, H-3), 5.19–5.01 (m, 6H, o-$C_6H_4(CH_2O)_2$P and –OCH_2–$COOCH_2$–C_6H_5), 4.89 (d, J = 3.3 Hz, 1H, H-1), 4.81 (d, J = 11.2 Hz, 1H, p-RCONH–C_6H_4–CH_2–), 4.61–4.54 (m, 11H, H-1′, H-4′, C_6H_5–CH_2–, p-CF_3–C_6H_4–CH_2–, p-RCONH–C_6H_4–CH_2–, and o-$C_6H_4(CH_2O)_2$P), 4.38 (d, J = 7.3 Hz, 2H, $(C_6H_4)_2$–CH–CH_2–OCO–), 4.30–4.20 (m, 5H, $(C_6H_4)_2$–CH–CH_2–OCO–, –OCH_2–$COOCH_2$–C_6H_5, and BA–CH_2–C_6H_4–CH_2NHCO–), 4.01 (dd, J = 13.2, 2.8 Hz, 1H, H-6′a), 3.84–3.80 (m, 4H, H-2, β-CH of 3-O-acyl and 3′-O-acyl, and β-CH of 2′-N-acyl), 3.75–3.72 (m, 3H, H-4, H-6a, and H-5′), 3.68–3.65 (m, 2H, H-2′ and H-6′b), 3.45–3.41 (m, 2H, H-5 and H-6b), 3.08 (s, 2H, BA–CH_2–C_6H_4–CH_2NHCO–), 2.65 (dd, J = 15.0, 5.5 Hz, 1H, α-CH_2 of 3-O-acyl), 2.53–2.44 (m, 2H, α-CH_2 of 3-O-acyl and 3′-O-acyl), 2.40 (dd, J = 15.0, 5.6 Hz, 1H, α-CH_2 of 3′-O-acyl), 2.30 (dd, J = 6.3, 6.3 Hz, 2H, –CO–CH_2–CH_2–CH_2–CO–), 2.28 (dd, J = 14.5, 7.0 Hz, 2H, α-CH_2 of 2′-N-acyl's side chain), 2.21 (dd, J = 16.5, 8.5 Hz, 2H, α-CH_2 of 2′-N-acyl's main chain), 2.17 (dd, J = 6.3, 6.3 Hz, 2H, –CO–CH_2–CH_2–CH_2–CO–), 1.97 (q, J = 7.3 Hz, 2H, –CH_2–CH_3 of BA), 1.92 (dd, J = 6.3, 6.3 Hz, 2H, –CO–CH_2–CH_2–CH_2–CO–), 1.55–1.01 (m, 54H, CH_2 × 27), 0.88–0.72 (m, 15H, –CH_2–CH_3 × 5).

47b: In a manner similar to the synthesis of **47a**, **46b** (111 mg, 49.8 μmol) was deprotected and acylated with (*R*)-3-(4-trifluoromethylbenzyloxy)decanoic acid (**20**) to yield **47b** as a pale yellow solid (54.5 mg, 44%). ESI-MS (positive) m/z 2468.98 $[M+H]^+$, 2489.97 $[M+Na]^+$.

47c: In a manner similar to the synthesis of **47a**, **46b** (110 mg, 49.7 μmol) was deprotected and acylated with (*R*)-3-(dodecanoyloxy)decanoic acid (**21**) to yield **47c** as a pale yellow solid (65.9 mg, 53%). ESI-MS (positive) m/z 2492.93 $[M+H]^+$, 2514.23 $[M+Na]^+$.

47d: In a manner similar to the synthesis of **47a**, **46c** (59.6 mg, 26.5 μmol) was deprotected and acylated with (*R*)-3-(4-trifluoromethylbenzyloxy)decanoic acid (**20**) to yield **47d** as a pale yellow solid (24.5 mg, 37%). ESI-MS (positive) m/z 1244.15 $[M+2H]^{2+}$.

47e: In a manner similar to the synthesis of **47a**, **46d** (78.0 mg, 35.1 μmol) was deprotected and acylated with (*R*)-3-(4-trifluoromethylbenzyloxy)decanoic acid (**20**) to yield **47e** as a pale yellow solid (41.2 mg, 42%). ESI-MS (positive) m/z 2469.18 $[M+H]^+$, 2489.74 $[M+Na]^+$, 1245.40 $[M+H+Na]^{2+}$, 1256.35 $[M+2Na]^{2+}$.

47f: In a manner similar to the synthesis of **47a**, **46d** (78.0 mg, 35.1 μmol) was deprotected and acylated with (*R*)-3-(dodecanoyloxy)decanoic acid (**21**) to yield **47f** as a pale yellow solid (67.4 mg, 63%). ESI-MS (positive) m/z 2515.20 $[M+Na]^+$, 1256.95 $[M+H+Na]^{2+}$, 1268.40 $[M+2Na]^{2+}$.

2-,2′-N-,3-,3′-O-Tetraacylated Compounds 30a, 30b, 30c, 30d, 30e, and 30f. 30a: To a solution of **47a** (38.0 mg, 15.4 μmol) in CH_2Cl_2 (2.0 mL) was added DBU (2.5 μL, 16.7 μmol) at room temperature and the mixture was stirred for 1.5 h. The reaction mixture was directly subjected to silica-gel column chromatography (5.0 g, $CHCl_3$:MeOH = 10:1) to give 2-N-deprotected product as a colorless solid: Yield 19.0 mg (63%). To a solution of the 2-N-free product and (*R*)-3-(dodecanoyloxy)-decanoic acid (**21**) (28.0 mg, 75.6 μmol) in anhydrous CH_2Cl_2 (2.0 mL) were added DIC (25.0 μL, 160 μmol) at room temperature under Ar atmosphere. After stirring for 14 h, to the reaction mixture was added toluene (2.0 mL) and the mixture was subjected to affinity separation (13 g × 1) to give **30a** as a pale yellow solid (18.7 mg, 49%). ESI-MS (positive) m/z 2620.88 $[M+Na]^+$, 1321.05 $[M+2Na]^{2+}$. ^{1}H NMR (400 MHz, DMSO-d_6, 40 °C): δ 9.81 (s, 1H, NH), 8.25 (s, 1H, NH), 7.65 (dd, J = 8.5, 7.3 Hz, 2H, –OCH_2–$COOCH_2$–C_6H_5), 7.55 (d, J = 7.3 Hz, 4H, p-CF_3–C_6H_4–CH_2–), 7.35–7.29 (m, 12H, p-RCONH–C_6H_4–CH_2–, p-CF_3–C_6H_4–CH_2–, and C_6H_5–CH_2–), 7.26–7.20 (m, 7H, BA–CH_2–C_6H_4–CH_2NHCO–, o-$C_6H_4(CH_2O)_2$P–, and –OCH_2–$COOCH_2$–C_6H_5), 7.16 (d, J = 7.8 Hz, 2H, BA–CH_2–C_6H_4–CH_2NHCO–), 7.02 (d, J = 7.8 Hz, 2H, p-RCONH–C_6H_4–CH_2–), 6.39 (d, J = 8.3 Hz, 1H, 2′-NH), 6.20 (d, J = 7.3 Hz, 1H, 2-NH), 5.60 (d, J = 6.5 Hz, 1H, NH), 5.48 (dd, J = 10.5, 9.3 Hz, 1H, H-3′), 5.36 (dd, J = 10.5, 10.5 Hz, 1H, H-3), 5.23–5.01 (m, 6H, o-$C_6H_4(CH_2O)_2$P and –OCH_2–$COOCH_2$–C_6H_5), 4.85 (d, J = 3.5 Hz, 1H, H-1), 4.75 (d, J = 10.5 Hz, 1H, p-RCONH–C_6H_4–CH_2–), 4.62–4.50 (m, 11H, H-1′, H-4′, C_6H_5–CH_2–, p-CF_3–C_6H_4–CH_2–, p-RCONH–C_6H_4–CH_2–, and o-$C_6H_4(CH_2O)_2$P), 4.33–4.20 (m, 4H, –OCH_2–$COOCH_2$–C_6H_5 and BA–CH_2–C_6H_4–CH_2NHCO–), 4.01 (dd, J = 13.2, 1.8 Hz, 1H, H-6′a), 3.88–3.79 (m, 4H, H-2, β-CH of 3-O-acyl and 3′-O-acyl, and β-CH of 2′-N-acyl), 3.75–3.72 (m, 5H, H-4, H-6a, H-5′, H-6′b, and β-CH of 2-N-acyl), 3.68–3.64 (m, 2H, H-2′ and H-6′b), 3.45–3.40 (m, 2H, H-5 and H-6b), 3.12 (d, J = 3.1 Hz, 2H, BA–CH_2–C_6H_4–CH_2NHCO–), 2.65 (dd, J = 15.1, 5.5 Hz, 1H, α-CH_2 of 3-O-

acyl), 2.53–2.43 (m, 2H, α-CH_2 of 3-*O*-acyl and 3′-*O*-acyl), 2.40 (dd, $J = 15.0$, 5.6 Hz, 1H, α-CH_2 of 3′-*O*-acyl), 2.31 (dd, $J = 7.0$, 7.0 Hz, 2H, –CO–CH_2–CH_2–CH_2–CO–), 2.28–2.20 (m, 8H, α-CH_2 of 2′-*N*-acyl's main and side chains, and α-CH_2 of 2′-*N*-acyl's main and side chains), 2.16 (dd, $J = 7.0$, 7.0 Hz, 2H, –CO–CH_2–CH_2–CH_2–CO–), 2.08 (q, $J = 6.9$ Hz, 2H, –CH_2–CH_3 of BA), 1.97 (dd, $J = 7.0$, 7.0 Hz, 2H, –CO–CH_2–CH_2–CH_2–CO–), 1.61–1.43 (m, 12H, γ-CH_2 of 2-*N*-acyl, 2′-*N*-acyl, 3-*O*-acyl, and 3′-*O*-acyl), 1.35–1.08 (m, 76H, –CH_2– × 38), 0.88 (t, $J = 6.9$ Hz, 21H, –CH_2–CH_3 × 7).

30b: In a manner similar to the synthesis of **30a**, **47b** (55.0 mg, 22.3 μmol) was deprotected and acylated with (*R*)-3-(dodecanoyloxy)decanoic acid (**21**) to yield **16b** as a pale yellow solid: Yield 19.7 mg (39%); ESI-MS (positive) m/z 2622.53 $[M + Na]^+$.

30c: In a manner similar to the synthesis of **30a**, **47c** (66.0 mg, 26.8 μmol) was deprotected and acylated with (*R*)-3-(4-trifluoromethylbenzyloxy)decanoic acid (**20**) to yield **30c** as a pale yellow solid (17.9 mg, 35%). ESI-MS (positive) m/z 2620.30 $[M + Na]^+$, 1299.57 $[M + 2H]^{2+}$.

30d: In a manner similar to the synthesis of **30a**, **47d** (24.7 mg, 9.91 μmol) was deprotected and acylated with (*R*)-3-(4-trifluoromethylbenzyloxy)decanoic acid (**20**) to yield **30d** as a pale yellow solid (3.3 mg, 14%). ESI-MS (positive) m/z 2621.46 $[M + Na]^+$, 1311.14 $[M + H + Na]^{2+}$, 1321.56 $[M + 2Na]^{2+}$.

30e: In a manner similar to the synthesis of **30a**, **47e** (42.7 mg, 17.3 μmol) was deprotected and acylated with (*R*)-3-(dodecanoyloxy)decanoic acid (**21**) to yield **30e** as a pale yellow solid (5.2 mg, 12%). ESI-MS (positive) m/z 2620.55 $[M + Na]^+$, 1311.06 $[M + H + Na]^{2+}$, 1321.42 $[M + 2Na]^{2+}$.

30f: In a manner similar to the synthesis of **30a**, **47f** (68.4 mg, 27.4 μmol) was deprotected and acylated with (*R*)-3-(4-trifluoromethylbenzyloxy)decanoic acid (**20**) to yield **30f** as a pale yellow solid (3.0 mg, 6.0%). ESI-MS (positive) m/z 1312.33 $[M + H + Na]^{2+}$, 1321.77 $[M + 2Na]^{2+}$.

CM-Analogues 26a, 26b, 26c, 26d, 26e, and 26f. 2-Deoxy-6-*O*-[2-deoxy-2-((*R*)-3-(dodecanoyloxy)decanoylamino)-3-*O*-((*R*)-3-hydroxydecanoyl)-4-*O*-phosphono-β-D-glucopyranosyl]-2-((*R*)-3-(dodecanoyloxy)decanoylamino)-3-*O*-((*R*)-3-hydroxydecanoyl)-α-D-glucopyranosyloxyacetic Acid (26a): To a solution of **30b** (18.0 mg, 6.93 μmol) in THF–AcOH (3:1) (2.4 mL) was added $Pd(OH)_2$ (25.0 mg). The mixture was stirred under 19 kg cm^{-2} of hydrogen at room temperature for 1 d. After removal of the Pd catalyst by filtration, the solvent was evaporated in vacuo. The crude product was purified by liquid–liquid partition column chromatography (5.0 g of Sephadex® LH-20, $CHCl_3$:MeOH:water:*i*-PrOH = 10:10:10:1.3). The organic layer was the stationary phase, and the aqueous layer was the mobile phase in this chromatography. After removal of the solvent in vacuo, the residue was lyophilized from sterilized water to afford **26a** as a colorless solid (4.0 mg, 60%). ESI-MS (negative) m/z 1521.77 $[M - H]^-$, 760.35 $[M - 2H]^{2-}$. ^1H NMR (600 MHz, $CDCl_3$:MeOH-d_4 = 1:1) δ 5.20–5.04 (m, 2H, β-CH of 2-*N*-acyl and 2′-*N*-acyl), 5.19 (dd, $J = 8.7$, 8.7 Hz, 1H, H-3), 5.14 (dd, $J = 8.9$, 8.9 Hz, 1H, H-3′), 4.74 (d, $J = 3.1$ Hz, 1H, H-1), 4.66 (d, $J = 7.4$ Hz, 1H, H-1′), 4.20–4.16 (m, 2H, H-2′ and H-4′), 4.03 (d, $J = 12.3$ Hz, 1H, –OCH_2–COOH), 4.01–3.96 (m, 3H, H-6a, H-6′a, and β-CH of 3′-*O*-acyl), 3.83 (d, $J = 12.3$ Hz, 1H, –OCH_2–COOH), 3.81–3.68 (m, 5H, H-2′, H-5, H-6b, H-6′b, and β-CH of 3-*O*-acyl), 3.56 (dd, $J = 8.7$, 8.7 Hz, 1H, H-4), 3.46 (dd, $J = 6.9$, 6.9 Hz, 1H, H-5′), 2.45 (dd, $J = 12.8$, 6.3 Hz, 1H, α-CH_2 of 2′-*N*-acyl's main chain), 2.38 (dd, $J = 12.9$, 3.8 Hz, 1H, α-CH_2 of 2-*N*-acyl's main chain), 2.28–2.21 (m, 10H, α-CH_2 of 3-*O*-acyl, 3′-*O*-acyl, 2-*N*-acyl's main and side chain, and 2′-*N*-acyl's main and side chain), 1.60–1.52 (m, 8H, γ-CH_2 of 3-*O*-acyl, 3′-*O*-acyl, 2-*N*-acyl's main chain, and 2′-*N*-acyl's main chain), 1.31–1.16 (m, 66H, –CH_2– × 33), 0.85 (t, $J = 6.6$ Hz, 18H, –CH_3 × 6).

26b: In a manner similar to the synthesis of **26a**, **30b** (18.0 mg, 6.93 μmol) was hydrogenolytically deprotected to give **26b** as a colorless solid (2.7 mg, 25%). ESI-MS (negative) m/z 1521.24 $[M - H]^-$, 760.26 $[M - 2H]^{2-}$.

26c: In a manner similar to the synthesis of **26a**, **30c** (17.0 mg, 6.54 μmol) was hydrogenolytically deprotected to give **26c** as a colorless solid (2.1 mg, 22%). ESI-MS (negative) m/z 1521.54 $[M - H]^-$, 760.39 $[M - 2H]^{2-}$.

26d: In a manner similar to the synthesis of **26a**, **30d** (3.3 mg, 1.27 μmol) was hydrogenolytically deprotected to give **26d** as a colorless solid (1.3 mg, 67%). ESI-MS (negative) m/z 761.23 $[M - 2H]^{2-}$.

26e: In a manner similar to the synthesis of **26a**, **30e** (5.2 mg, 2.00 μmol) was hydrogenolytically deprotected to give **26e** as a colorless solid (1.7 mg, 56%). ESI-MS (negative) m/z 1522.11 $[M - H]^-$, 760.46 $[M - 2H]^{2-}$.

26f: In a manner similar to the synthesis of **26a**, **30f** (3.8 mg, 1.46 μmol) was hydrogenolytically deprotected to give **26f** as a colorless solid (1.5 mg, 67%). ESI-MS (negative) m/z 1521.93 $[M - H]^-$, 760.44 $[M - 2H]^{2-}$.

***Limulus* Assay.** *Limulus* activity of synthetic samples were measured by means of the Endospecy Test® (Seikagaku Kogyo, Tokyo, Japan) using an LPS specimen from *E. coli* O111:B1 (Sigma-Aldrich Chemical Co.) as a reference standard. A solution of a test sample in 1% DMSO in distilled water (30 μL) was mixed with the reagent in the Endospecy ES-50M set (30 μL) and incubated in duplicate in a 96-well plastic plate (Toxipet plate 96F, Seikagaku Kogyo) at 37 °C for 30 min. Sodium nitrate (75 μL, 0.04% in 0.48 mol dm^{-3} hydrochloric acid), 75 μL of 0.3% ammonium sulfate, and 75 μL of 0.07% *N*-1-naphthylethylenediamine dichloride were added successively. The absorbance at 414 nm of each well was measured using a micro plate reader.

***Cytokine* Assay.** Heparinized human whole blood diluted with RPMI 1640 (Biken, Osaka, Japan) (v/v, 1/4) was incubated at 37 °C for 24 h in humidified air containing 5% (v/v) CO_2 in a 96-well culture plate (Becton Dickson) with or without various doses of test specimens for interleukin-6 (IL-6) assay. The amounts of cytokine induced were measured from the culture supernatants using the appropriate ELISA kit systems (IL-6 and TNF-α, ELISA Development Kit human IL-6 and ELISA Development Kit human TNF-α, Genzyme TECHNE Co., Minneapolis, MN, USA). These assays were performed according to the manufacturer's instructions, and the cytokine amount was determined from a standard curve prepared for each assay. Assays were repeated three times. Similar results were obtained in repeated experiments.

This work was supported in part by Grants-in-Aid for Scientific research (Nos. 14380288, 15310149, 17035050, 17310128, and 18032046) from the Japan Society for the Promotion of Science, the Grant-in-Aid for Creative Scientific Research "In vivo Molecular Science for Discovery of New Biofunctions and Pharmaceutical Drugs" No. 13NP0401 from the Ministry of Education, Culture, Sports, Science and Technology of Japan; and grants from Suntory Institute for Bioorganic Research (SUNBOR Grant), the Houansha Foun-

dation, and Hayashi Memorial Foundation for Female Natural Scientists (to YF). We are grateful to Prof. T. Tamura and Ms. K. Aoyama at Hyogo medical college for their assistance in the cytokine induction assay.

References

1 S. Akira, S. Uematsu, O. Takeuchi, *Cell* **2006**, *124*, 783.

2 E. Meylan, J. Tschopp, M. Karin, *Nature* **2006**, *442*, 39.

3 J. H. Fritz, S. E. Girardin, *J. Endotoxin Res.* **2005**, *11*, 390.

4 B. Pulendran, K. Palucka, J. Banchereau, *Science* **2001**, *293*, 253.

5 A. Aderem, R. J. Ulevitch, *Nature* **2000**, *406*, 782.

6 *Endotoxin in Health and Disease*, ed. by H. Brade, S. M. Opal, S. N. Vogel, D. C. Morrison, Marcel Dekker, Inc., NewYork, Basel, **1999**.

7 B. Beutler, E. T. Rietschel, *Nat. Rev. Immunol.* **2003**, *3*, 169.

8 C. Alexander, E. T. Rietschel, *J. Endotoxin Res.* **2001**, *7*, 167.

9 A. J. Ulmer, E. Th. Rietschel, U. Zähringer, H. Heine, *Trends Glycosci. Glycotechnol.* **2002**, *14*, 53.

10 C. Alexander, U. Zähringer, *Trends Glycosci. Glycotechnol.* **2002**, *14*, 69.

11 S. Kusumoto, K. Fukase, *Chem. Rec.* **2006**, *6*, 333.

12 S. Saitoh, K. Miyake, *Chem. Rec.* **2006**, *6*, 311.

13 a) M. Imoto, H. Yoshimura, M. Yamamoto, T. Shimamoto, S. Kusumoto, T. Shiba, *Tetrahedron Lett.* **1984**, *25*, 2667. b) M. Imoto, H. Yoshimura, M. Yamamoto, T. Shimamoto, S. Kusumoto, T. Shiba, *Bull. Chem. Soc. Jpn.* **1987**, *60*, 2197.

14 a) M. Imoto, H. Yoshimura, N. Sakaguchi, S. Kusumoto, T. Shiba, *Tetrahedron Lett.* **1985**, *26*, 1545. b) M. Imoto, H. Yoshimura, T. Shimamoto, N. Sakaguchi, S. Kusumoto, T. Shiba, *Bull. Chem. Soc. Jpn.* **1987**, *60*, 2205.

15 E. T. Rietschel, H. Brade, O. Holst, L. Brade, S. Müler-Loennings, U. Mamat, U. Zähringer, F. Beckmann, U. Seydel, K. Brandenburg, A. J. Ulmer, T. Mattern, H. Heine, J. Schletter, H. Loppnow, U. Schönbeck, H.-D. Flad, S. Hauschildt, U. F. Schade, F. D. Padova, S. Kusumoto, R. R. Schumann, in *Pathology of Septic Shock* in *Current Topics in Microbiology and Immunology*, ed. by E. T. Rietschel, H. Wagner, Springer-Verlag, Berlin Heidelberg, **1996**, Vol. 216, pp. 39–81.

16 H. Loppnow, H. Brade, I. Durrbaum, C. A. Dinarello, S. Kusumoto, E. T. Rietschel, H.-D. Flad, *J. Immunol.* **1989**, *142*, 3229.

17 E. T. Rietschel, T. Kirikae, F. U. Schade, A. J. Ulmer, O. Holst, H. Brade, G. Schmidt, U. Mamat, H.-D. Grimmecke, S. Kusumoto, U. Zähringer, *Immunobiology* **1993**, *187*, 169.

18 a) T. 'Kusama, T. Soga, E. Shioya, K. Nakayama, H. Nakajima, Y. Osada, Y. Ono, S. Kusumoto, T. Shiba, *Chem. Pharm. Bull.* **1990**, *38*, 3366. b) A. J. Ulmer, A. H. Heine, W. Feist, S. Kusumoto, T. Kusama, H. Brade, U. Schade, E. T. Rietschel, H.-D. Flad, *Infect. Immun.* **1992**, *60*, 3309.

19 T. Kusama, T. Soga, Y. Ono, E. Kumazawa, E. Shioya, K. Nakayama, K. Uoto, Y. Osada, *Chem. Pharm. Bull.* **1991**, *39*, 3244.

20 W.-C. Liu, M. Oikawa, K. Fukase, Y. Suda, S. Kusumoto, *Bull. Chem. Soc. Jpn.* **1999**, *72*, 1377.

21 K. Fukase, A. Ueno, Y. Fukase, M. Oikawa, Y. Suda, S. Kusumoto, *Bull. Chem. Soc. Jpn.* **2003**, *76*, 485.

22 a) R. L. Delude, R. Savedra, Jr., H. Zhao, R. Thieringer, S. Yamamoto, M. J. Fenton, D. T. Golenbock, *Proc. Natl. Acad. Sci. U.S.A.* **1995**, *92*, 9288. b) D. T. Golenbock, R. Y. Hampton, N. Qureshi, K. Takayama, C. R. H. Raetz, *J. Biol. Chem.* **1991**, *266*, 19490. c) P. V. Salimath, J. Weckesser, W. Strittmatter, H. Mayer, *Eur. J. Biochem.* **1983**, *136*, 195.

23 W. J. Christ, O. Asano, A. L. Robidoux, M. Perez, Y. Wang, G. R. Dubuc, W. E. Gavin, L. D. Hawkins, P. D. McGuinness, M. A. Mullarkey, M. D. Lewis, Y. Kishi, T. Kawata, J. R. Bristol, J. R. Rose, D. P. Rossignol, S. Kobayashi, I. Hishinuma, A. Kimura, N. Asakawa, K. Katayama, I. Yamatsu, *Science* **1995**, *268*, 80.

24 D. P. Rossignol, M. Lynn, *J. Endotoxin Res.* **2002**, *8*, 483.

25 K. Fukase, Y. Fukase, M. Oikawa, W.-C. Liu, Y. Suda, S. Kusumoto, *Tetrahedron* **1998**, *54*, 4033.

26 Y. Zhang, J. Gaekwad, M. A. Wolfert, G. J. Boons, *J. Am. Chem. Soc.* **2007**, *129*, 5200.

27 a) H. Masoud, B. Lindner, J. Weckesser, H. Meyer, *Syst. Appl. Microbiol.* **1990**, *13*, 227. b) U. Seydel, M. Oikawa, K. Fukase, S. Kusumoto, K. Brandenburg, *Eur. J. Biochem.* **2000**, *267*, 3032.

28 a) H. W. Wollenweber, U. Seydel, B. Lindner, O. Lüderitz, E. T. Rietschel, *Eur. J. Biochem.* **1984**, *145*, 265. b) A. B. Schromm, K. Brandenburg, H. Loppnow, A. P. Moran, M. H. Koch, E. T. Rietschel, U. Seydel, *Eur. J. Biochem.* **2000**, *267*, 2008.

29 H. Yoshizaki, N. Fukuda, K. Sato, M. Oikawa, K. Fukase, Y. Suda, S. Kusumoto, *Angew. Chem., Int. Ed.* **2001**, *40*, 1475.

30 R. R. Schmidt, W. Kinzy, *Advances in Carbohydrate Chemistry and Biochemistry*, Elsevier, **1994**, Vol. 50, p. 21.

31 Y. Fukase, S.-Q. Zhang, K. Iseki, M. Oikawa, K. Fukase, S. Kusumoto, *Synlett* **2001**, 1693.

32 K. Fukase, S.-Q. Zhang, Y. Fukase, N. Umesako, S. Kusumoto, *ACS Symp. Ser.* **2005**, *92*, 87.

33 Y. Sakai, M. Oikawa, H. Yoshizaki, T. Ogawa, Y. Suda, K. Fukase, S. Kusumoto, *Tetrahedron Lett.* **2000**, *41*, 6843.

34 S. D. Debenham, E. J. Toone, *Tetrahedron: Asymmetry* **2000**, *11*, 385.

35 Y. Watanabe, Y. Komoda, K. Ebisuya, S. Ozaki, *Tetrahedron Lett.* **1990**, *31*, 255.

36 J. J. Oltvoort, C. A. A. v. Boeckel, J. H. d. Koning, J. H. v. Boom, *Synthesis* **1981**, 305.

37 F. J. Urban, B. S. Moore, R. Breitenbach, *Tetrahedron Lett.* **1990**, *31*, 4421.

38 Y. Suda, H. Tochio, K. Kawano, H. Takada, T. Yoshida, S. Kotani, S. Kusumoto, *FEMS Immunol. Med. Microbiol.* **1995**, *12*, 97.

39 K. Fukase, M. Oikawa, Y. Suda, W.-C. Liu, Y. Fukase, T. Shintaku, H. Sekljic, H. Yoshizaki, S. Kusumoto, *J. Endotoxin Res.* **1999**, *5*, 46.

40 U. Seydel, A. B. Schromm, L. Brade, S. Gronow, J. Andra, M. Muller, M. H. Koch, K. Fukase, M. Kataoka, M. Hashimoto, S. Kusumoto, K. Brandenburg, *FEBS J.* **2005**, *272*, 327.

41 M. Kataoka, M. Hashimoto, Y. Suda, S. Kusumoto, K. Fukase, *Hetrocycles* **2006**, *69*, 395.

42 S. Kotani, H. Takada, M. Tsujimoto, T. Ogawa, I. Takahashi, T. Ikeda, K. Otsuka, H. Shimauchi, N. Kasai, J. Mashimo, *Infect. Immun.* **1985**, *49*, 225.

43 a) S.-Q. Zhang, K. Fukase, S. Kusumoto, *Tetrahedron Lett.* **1999**, *40*, 7479. b) S.-Q. Zhang, K. Fukase, S. Kusumoto, in *Peptide Science 1999*, ed. by N. Fujii, The Japanese Peptide Society, **2000**, pp. 151–154.

44 K. Fukase, M. Takashina, Y. Hori, D. Tanaka, K. Tanaka, S. Kusumoto, *Synlett* **2005**, 2342.

45 S.-Q. Zhang, K. Fukase, M. Izumi, Y. Fukase, S. Kusumoto, *Synlett* **2001**, 590.

46 a) Y. Fukase, K. Fukase, S. Kusumoto, *Tetrahedron Lett.* **1999**, *40*, 1169. b) Y. Fukase, K. Fukase, S. Kusumoto, in *Peptide Science 1999*, ed. by N. Fujii, The Japanese Peptide Society, **2000**, pp. 93–96.

47 a) K. Iijima, W. Fukuda, M. Tomoi, *J. Macromol. Sci., Pure Appl. Chem.* **1992**, *29*, 249. b) W. Xu, R. Mohan, M. Morrissey, *Bioorg. Med. Chem. Lett.* **1998**, *8*, 1089. c) W. Xu, R. Mohan, M. Morrissey, *Tetrahedron Lett.* **1997**, *38*, 7337.

48 a) M. Isobe, Y. Ichikawa, D.-L. Bai, H. Masaki, T. Goto, *Tetrahedron* **1987**, *43*, 4767. b) M. Isobe, Y. Ichikawa, T. Goto, *Tetrahedron Lett.* **1986**, *27*, 963.

49 E. Haslam, *Tetrahedron* **1980**, *36*, 2409.

50 J. Lee, J. H. Griffin, T. I. Nicas, *J. Org. Chem.* **1996**, *61*, 3983.

51 M. Azuma, A. Matsuo, Y. Fujimoto, K. Fukase, K. Hazeki, O. Hazeki, M. Matsumoto, T. Seya, *Biochem. Biophys. Res. Commun.* **2007**, *354*, 574.

52 U. Ohto, K. Fukase, K. Miyake, Y. Satow, *Science* **2007**, *316*, 1632.

53 H. M. Kim, B. S. Park, J.-I. Kim, S. E. Kim, J. Lee, S. C. Oh, P. Enkhbayar, N. Matsushima, H. Lee, O. J. Yoo, J.-O. Lee, *Cell* **2007**, *130*, 906.

54 M. Mueller, B. Lindner, S. Kusumoto, K. Fukase, A. B. Schromm, U. Seydel, *J. Biol. Chem.* **2004**, *279*, 26307.

55 S. Saitoh, S. Akashi, T. Yamada, N. Tanimura, M. Kobayashi, K. Konno, F. Matsumoto, K. Fukase, S. Kusumoto, Y. Nagai, Y. Kusumoto, A. Kosugi, K. Miyake, *Int. Immunol.* **2004**, *16*, 961.

56 S. Saitoh, S. Akashi, T. Yamada, N. Tanimura, F. Matsumoto, K. Fukase, S. Kusumoto, A. Kosugi, K. Miyake, *J. Endotoxin Res.* **2004**, *10*, 257.

57 M. Kobayashi, S. Saitoh, N. Tanimura, K. Takahashi, K. Kawasaki, M. Nishijima, Y. Fujimoto, K. Fukase, S. Akashi-Takamura, K. Miyake, *J. Immunol.* **2006**, *176*, 6211.

58 M. Akamatsu, Y. Fujimoto, M. Kataoka, Y. Suda, S. Kusumoto, K. Fukase, *Bioorg. Med. Chem.* **2006**, *14*, 6759.

59 Y. Fujimoto, Y. Adachi, M. Akamatsu, Y. Fukase, M. Kataoka, Y. Suda, K. Fukase, S. Kusumoto, *J. Endotoxin Res.* **2005**, *11*, 341.

60 Y. Fujimoto, M. Iwata, N. Imakita, A. Shimoyama, Y. Suda, S. Kusumoto, K. Fukase, *Tetrahedron Lett.* **2007**, *48*, 6577.

9

Age-related maculopathy and sunlight exposure evaluated by objective measurement

M Hirakawa, M Tanaka, Y Tanaka, A Okubo, C Koriyama, M Tsuji, S Akiba, K Miyamoto, G Hillebrand, T Yamashita and T Sakamoto

Br. J. Ophthalmol. 2008;92;630-634
doi:10.1136/bjo.2007.130575

Age-related maculopathy and sunlight exposure evaluated by objective measurement

M Hirakawa,[1] M Tanaka,[1] Y Tanaka,[1] A Okubo,[1] C Koriyama,[2] M Tsuji,[2] S Akiba,[2] K Miyamoto,[3] G Hillebrand,[3] T Yamashita,[1] T Sakamoto[1]

[1] Department of Ophthalmology, Kagoshima University Graduate School of Medical and Dental Sciences, Kagoshima, Japan; [2] Department of Epidemiology and Preventive Medicine, Kagoshima University Graduate School of Medical and Dental Sciences, Kagoshima, Japan; [3] Procter & Gamble, Kobe, Japan

Correspondence to: Dr T Sakamoto, Department of Ophthalmology, Kagoshima University Graduate School of Medical and Dental Sciences, 8-35-1 Sakuragaoka, Kagoshima 890-8520, Japan; tsakamot@m3.kufm.kagoshima-u.ac.jp

Accepted 11 January 2008

ABSTRACT

Aim: To study the relationship between age-related maculopathy (ARM) and exposure to sunlight using an objective method.

Methods: In a case–control study of Japanese men aged ≥50 years (67 controls without ophthalmic disease and 148 with ARM), those with ARM were separated into groups of early (n = 75) and late (n = 73) ARM. Facial wrinkle length and area of hyperpigmentation, which are considered to be associated with exposure to sun, were measured using imaging with computer-based image analysis. Skin tone was also measured on the upper inner arm, which is not exposed to sun. Early and late ARM association with skin measurements was then evaluated.

Results: Significantly more facial wrinkling ($p = 0.047$, odds ratio 3.8; 95% CI 1.01 to 13.97) and less facial hyperpigmentation ($p = 0.035$, odds ratio 0.3; 95% CI 0.08 to 0.92) was present in late ARM cases. The relationship between skin tone and ARM risk was not statistically significant.

Conclusions: This objective method showed that lifetime exposure to sunlight is an important factor in the progression of late ARM. An individual's reaction to sunlight exposure may have a role in ARM progression in addition to total lifetime exposure to sunlight.

The aetiology of age-related maculopathy (ARM), which is the most common cause of vision loss in older people in developed countries, remains unclear, but is suspected to involve both external and internal factors.[1–7] Of the external factors, smoking is the most well-established independent risk factor.[4–7] In contrast, there is controversy over the role of other potential external factors, such as exposure to sunlight or ultraviolet radiation (UV).[8–16] It has been reported that abnormal skin sensitivity to sunlight or a propensity to tan is associated with ARM.[11–13] However, there are several reports that sunlight exposure is not a risk factor related to ARM.[14–17]

The controversy is probably due to the methods used to measure lifetime exposure to sunlight. Most studies assessed total sunlight exposure by using questionnaires, and the accuracy of the data obtained depends heavily on question "quality" and respondents' memory. This is an inevitable and unsolvable problem of questionnaire methodology.[8–17]

We previously reported[18 19] that people with different lifetime exposures to sunlight have correspondingly different severities of facial skin wrinkling and hyperpigmentation. In those earlier studies, we used video imaging combined with image analysis to objectively quantify skin features, reasoning that wrinkling and hyperpigmentation were quantitative, objective biomarkers of the exposure of people of the same gender and ethnic group, and thus measured true lifetime exposure more accurately than questionnaires. We used these measurements to evaluate the relationship between facial wrinkling and hyperpigmentation and ARM.

SUBJECTS AND METHODS

This case–control study of ARM and healthy controls involved subjects seen at Kagoshima University Hospital or Kagoshima Kouseiren Hospital Health Care Center between May 2005 and February 2006 who met the inclusion criteria below, and were asked to participate after the study was carefully explained. Inclusion criteria were as follows:

1. Life-long residence in Kagoshima prefecture
2. Aged 50 years or older and male
3. Fundus photographs could be taken
4. Ocular fundi were observable
5. Absence of self-reported ocular disease, eg, glaucoma or diabetic retinopathy

Late ARM cases were those diagnosed at Kagoshima University Hospital during the study. Controls and early ARM cases had undergone health checks at Kagoshima Kouseiren Hospital Health Care Center during the same period.

An initial assessment of 259 participants excluded 44: 18 had media opacity and 26 had ocular diseases (four with diabetic retinopathy, one with branch retinal vein occlusion, three with glaucoma, five with epiretinal membrane, and 13 with polypoidal choroidal vasculopathy). The 215 subjects who met the inclusion criteria comprised 67 controls, 75 with early ARM and 73 with late ARM. All subjects with late ARM had neovascular membrane confirmed by angiography. No geographic atrophy was seen.

Our research followed the tenets of the Declaration of Helsinki, with informed consent obtained from the subjects, and was approved by all of the institutional review boards involved.

Fundus examination

Fundus colour photographs (45°) of the macula (Canon CR-DG10, Tokyo, Japan) were graded by two independent qualified judges (MH, AO), who had no contact with the subjects. ARM was defined on the basis of the International ARM Epidemiological Study Group classification[20]: early ARM by the presence of soft drusen (⩽63 μm) or retinal pigment epithelium pigmentation abnormalities within the grid, and late ARM by either

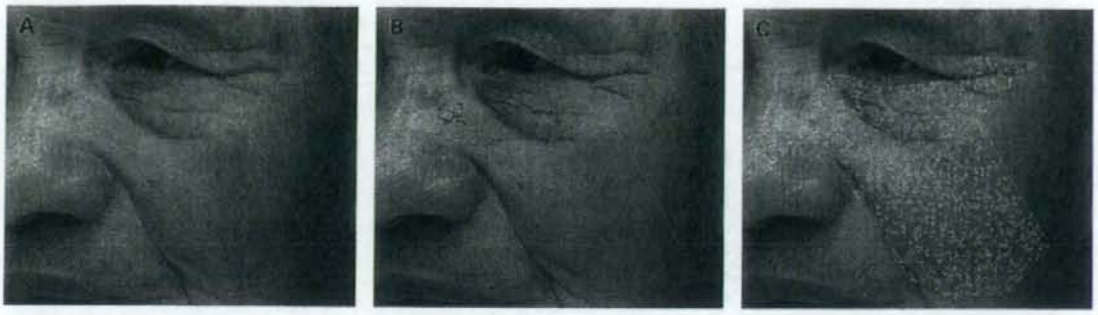

Figure 1 Representative images used to quantify facial wrinkling and hyperpigmentation. (A) The region of interest (ROI) was demarcated manually as shown by the green line. (B) The facial wrinkles detected in the ROI are shown (blue lines). (C) The hyperpigmented regions detected in the ROI are shown (yellow). Patient consent has been obtained for publication of this figure.

neovascular age-related macular degeneration or geographic atrophy involving the fovea. Minimum geographic atrophy was a circle of 175 μm or more in diameter. Those with fundus inflammatory or retinovascular disease, choroidal neovascularisation due to high myopia, or polypoidal choroidal vasculopathy confirmed by fluorescein and indocyanine green angiography were excluded. Classification was based on the subject's worst eye.

Smoking

Smoking history was obtained from questionnaires, with lifetime smoking exposure quantified in "pack-years", one "pack year" being 20 cigarettes smoked per day for one year.[21]

Hypertension

Blood pressure was measured three times with the subject in a sitting position, and the mean was used for analysis. Hypertension was defined as systolic blood pressure ≥140 mm Hg, diastolic blood pressure ≥90 mm Hg, or current use of antihypertensive drugs.

Skin examination

Wrinkles

The total length of facial wrinkles in the region of the upper cheek and temporal areas next to the eyes was objectively measured using a two-dimensional imaging system using a commercially available high-resolution digital camera equipped with a close-up lens mounted in a standardised illumination box fitted with head-positioning aids (Beauty Imaging System; Procter & Gamble, Cincinnati, Ohio, USA). The camera was calibrated daily using a GretagMacbeth neutral 8.0 grey colour board in front of the camera. Left and right views of the face were standardised—that is, the same focal distance from the camera lens to the face, same magnification, same head position so that the camera angle was the same relative to the face surface, and exactly the same lighting.[18 19 22 23] The region of interest (ROI) was marked manually based on 12 predefined facial landmarks around the eye and cheek—for example, corners of the eye, bridge of the nose, corners of the mouth (fig 1). The lengths of facial wrinkles (fine lines) in the ROI were quantified objectively using image analysis algorithms based on an Optimus software platform, which automatically locates each facial line and quantifies the total number, length and area of facial lines longer than 5 mm and more than 0.16 mm wide, known magnification used to convert pixel data to actual length and area data. Thresholds were based on "clinically important" wrinkling—that is, excluding lines shorter than 5 mm and narrower than 0.16 mm, which fall under the heading of surface "texture".

Because the ROI varies in shape and size, total wrinkle area was normalised to total ROI size to yield a wrinkle area fraction (WAF)—that is, fractional ROI area occupied by wrinkles or fine lines. WAF varied from 0.05 (5% of ROI) to 0.2 (20% of ROI) depending on individual severity of wrinkling. Group statistical analysis used the mean WAF on the left and right sides of the face for each subject. The intraindividual coefficient of variation of imaging (within-subject reproducibility) quantifying wrinkling was found previously to be 5.2%.[23] Accuracy was confirmed using mannequins with artificial wrinkles of known length and width. Imaging accuracy was ±5% of the actual value.[23]

Pigmentation

Total facial hyperpigmentation on the left and right sides was objectively measured using the Beauty Imaging System. The region hyperpigmentation was defined as a localised region of darker skin. Hyperpigmentation is often observed after inflammation, melasma and senile lentigines, and can be exacerbated by exposure to sun.[18 19] The ROI in each image was defined manually and then automatically analysed using customised software that locates and quantifies the total area of hyperpigmented spots. The total area of spots was then normalised to the total area of the region analysed. This analysis was conducted on both the left and right sides of the face, and the mean of the two sides was used as the final measure of hyperpigmentation for each subject in the group statistical analysis.

Skin tone

Skin tone was measured on the upper inner arm using a colour reader (CR-13; Minolta, Tokyo, Japan), which was calibrated using the standard white plates supplied with the instrument,[18 19 22] to obtain three skin tone indices L*, a* and b*, ie, lightness, redness and yellowness. Triplicate measurements at each site were averaged and analysed. Skin on the inner arm represents constitutive skin colour because it is not exposed to sun.

Table 1 Characteristics of study subjects

Characteristic	Control (n = 67)	Early ARM (n = 75)	Late ARM (n = 73)
Age (years)			
<60	25 (37.3)	7 (9.3)	5 (6.8)
60–64	11 (16.4)	10 (13.3)	5 (6.8)
65–69	12 (17.9)	18 (24.0)	14 (19.2)
70–74	17 (25.3)	26 (34.7)	14 (19.2)
≥75	2 (3.0)	14 (18.7)	35 (47.9)
Smoking (pack-years)			
0	32 (47.8)	37 (49.3)	11 (15.1)
1–24	16 (23.9)	14 (18.7)	25 (34.2)
≥25	19 (28.4)	24 (32.0)	37 (50.7)
Hypertension			
Absent	35 (52.2)	34 (45.3)	25 (34.2)
Present	32 (47.8)	41 (54.7)	48 (65.8)
Facial wrinkling			
<0.104	32 (47.8)	18 (24.0)	20 (27.4)
0.104–0.1314	20 (29.9)	29 (38.7)	22 (30.1)
≥0.1314	15 (22.4)	28 (37.3)	31 (42.5)
Facial hyperpigmentation			
<0.0264	19 (28.4)	20 (26.6)	31 (42.5)
0.0264–0.0342	24 (35.8)	27 (36.0)	20 (27.4)
≥0.0342	24 (35.8)	28 (37.3)	22 (30.1)
Upper inner arm skin tone L*			
<59.7	15 (22.4)	26 (34.7)	28 (38.4)
59.7–62.1	21 (31.3)	30 (40.0)	24 (32.9)
≥62.1	31 (46.3)	19 (25.3)	21 (28.8)
Upper inner arm skin tone a*			
<7.2	33 (49.3)	21 (28.0)	18 (24.7)
7.2–8.5	21 (31.3)	25 (33.3)	25 (34.2)
≥8.5	13 (19.4)	29 (38.7)	30 (41.1)
Upper inner arm skin tone b*			
<14.7	29 (43.3)	18 (24.0)	26 (35.6)?
14.7–16.7	19 (28.4)	24 (32.0)	24 (32.9)
≥16.7	19 (28.4)	33 (44.0)	23 (31.5)

Values are number (%).
ARM, age-related maculopathy.

Sample size

From previous work, the sun sensitivity index odds ratio (OR) for late ARM was 3,[13] so sample size was determined to detect ORs of 3.0 with 80% statistical power at $p \leq 0.05\%$. The required sample size was 66 in each group.

Statistical analysis

Stata 8.1 (Stata Corp, Lakeway Drive College Station, Texas, USA) was used for the statistical analysis. A multivariate logistic regression analysis obtained the maximum likelihood OR estimates and corresponding 95% CIs using ARM stage as a dependent variable. The possible risk factors, age, smoking and hypertension, and sun-related skin factors, facial wrinkling, facial hyperpigmentation and skin tone L*, a* and b*, were included in the models as covariates. Subjects were separated by age into the following groups: <60, 60–64, 65–69, 70–74 and ≥75. Smoking history was analysed as non-smoking, 0–24 pack-years and 25 pack-years or more. Hypertension was dichotomised into absence and presence. Each variable of the skin examination, wrinkling, hyperpigmentation and skin tone (L*, a* or b*), was divided into upper, middle and lower tertiles referenced in statistical analyses. Trend was analysed by a likelihood ratio test using categorical data as continuous variables. Two-sided $p<0.05$ was considered to be significant.

Table 2 Age, smoking status and hypertension in subjects with age-related maculopathy (ARM) compared with controls

Risk factor	Early ARM vs controls	Late ARM vs controls
Age (years)		
<60	1	1
60–64	3.7 (1.00 to 13.51)	2.8 (0.45 to 17.80)
65–69	5.3 (1.44 to 19.33)	9.7 (1.94 to 48.89)
70–74	5.7 (1.68 to 19.19)	7.3 (1.52 to 34.84)
≥75	25.1 (3.70 to 170.49)	114.5 (15.07 to 869.73)
p Value for trend	0.001	<0.001
Smoking (pack-years)		
0	1	1
0–25	1.2 (0.40 to 3.55)	5.2 (1.39 to 19.36)
≥25	0.9 (0.35 to 2.30)	5.4 (1.61 to 17.90)
p Value for trend	0.856	0.007
Hypertension		
Absent	1	1
Present	1.1 (0.51 to 2.48)	1.1 (0.41 to 3.18)
p Value	0.783	0.788

Values are OR (95% CI) adjusted for age, smoking, hypertension, facial wrinkling, facial hyperpigmentation and skin of upper inner arm (L*, a* or b*).

RESULTS

Study group baseline

Table 1 lists subjects on the basis of age, smoking status, hypertension, facial wrinkling, facial hyperpigmentation and skin tone.

Age

Mean (SD) age was 63.1 (8.1) years for the controls, 68.7 (6.9) years for the early ARM group, and 72.8 (7.9) years for the late ARM group. The early ARM ($p = 0.001$) and late ARM ($p<0.001$) groups were significantly older than the controls. Age was a significant factor related to both types of ARM (table 2).

Smoking

Smoking data (mean (SD)) were as follows: 16.1 (21.0) pack-years for controls, 17.8 (25.0) pack-years for the early ARM group, and 32.4 (29.0) pack-years for the late ARM group. Logistic regression analysis showed smoking to be significantly related to late ARM (p for trend = 0.007), but not early ARM (table 2).

Hypertension

Hypertension was not a significant risk for ARM groups (table 2).

Wrinkles

WAF increased with age in patients with ARM and controls (fig 2). However, the observed age dependence of WAF was not statistically significant in either patients or controls. Logistic analysis showed that patients with late ARM had larger WAFs on average than controls after adjustment for age, smoking, hypertension, facial hyperpigmentation and skin tone (p for trend = 0.047), but patients with early ARM did not (table 3).

Pigmentation

Facial pigmentation increased with age in patients with ARM and controls (fig 2). Here again the observed age dependence

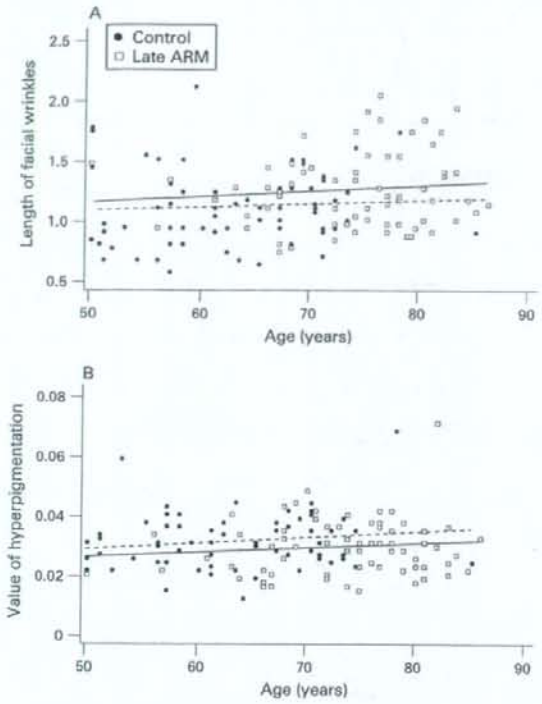

Figure 2 Facial wrinkling (A) and facial pigmentation (B) of patients with late age-related maculopathy (ARM) and controls according to age. (A) Regression lines were drawn separately for patients with late ARM (solid line: $y = 0.09168+0.00047x$) and controls (dotted line: $y = 0.08670+0.00040x$). (A) Wrinkle area fraction (WAF) increased with age in patients with late ARM and controls. However, the observed age dependence of WAF was not statistically significant in either patients or controls. (B) Regression lines were drawn separately for patients with late ARM (solid line: $y = 0.01898+0.00015x$) and controls (dotted line: $y = 0.02152+0.00016x$). Facial pigmentation increased with age in patients with late ARM and controls. However, the late ARM group was significantly less pigmented than the control group. Data for the early ARM group were not included to avoid overlapping of points.

was not significant in either patients or controls. Logistic analysis showed that patients with late ARM had smaller areas of pigmentation on average than controls after adjustment for age, smoking, wrinkling and upper inner arm skin (L*, a* and b*). In late ARM cases, a significantly smaller area of hyperpigmentation was found (p for trend = 0.035, table 3). There was no significant difference in area of hyperpigmentation between patients with early ARM and controls.

Skin tone

Mean (SD) indices of skin tone (L*, a* and b*) were: 61.9 (2.9), 7.6 (1.6) and 15.4 (2.6), respectively, for controls; 60.4 (2.3), 8.4 (1.9) and 16.3 (2.2), respectively, for early ARM; 60.4 (3.0), 8.3 (1.8) and 15.4 (2.6), respectively, for late ARM. Patients with ARM had darker, redder and more yellow skin, but no significant difference was seen in skin tone (L*, a* and b*) among the groups (table 3).

Table 3 Wrinkles, pigmentation and skin tone in subjects with age-related maculopathy (ARM) compared with controls

Risk factor	Early ARM vs controls	Late ARM vs controls
Facial wrinkling		
<0.104	1	1
0.104–0.1314	1.4 (0.53 to 3.49)	1.9 (0.54 to 6.56)
≥0.1314	2.5 (0.89 to 7.08)	3.8 (1.01 to 13.97)
p Value for trend	0.086	0.047
Facial hyperpigmentation		
<0.0264	1	1
0.0264–0.0342	0.6 (0.24 to 1.69)	0.3 (0.08 to 0.92)
≥0.0342	0.6 (0.21 to 1.56)	0.3 (0.08 to 0.92)
p Value for trend	0.332	0.035
Upper inner arm skin tone L*		
<59.7	1	1
59.7–62.1	0.9 (0.30 to 2.57)	0.5 (0.13 to 2.14)
≥62.1	0.9 (0.23 to 3.35)	0.6 (0.10 to 2.94)
p Value for trend	0.848	0.492
Upper inner arm skin tone a*		
<7.2	1	1
7.2–8.5	1.5 (0.51 to 4.37)	1.5 (0.38 to 5.64)
≥8.5	2.1 (0.58 to 7.69)	1.8 (0.37 to 9.17)
p Value for trend	0.257	0.120
Upper inner arm skin tone b*		
<14.7	1	1
14.7–16.7	1.1 (0.38 to 2.97)	0.7 (0.18 to 2.50)
≥16.7	1.2 (0.43 to 3.56)	0.3 (0.08 to 1.34)
p Value for trend	0.697	0.120

Values are OR (95% CI) obtained from the logistic model incorporating age, smoking, hypertension, facial wrinkling, facial hyperpigmentation and upper inner arm skin tone (L*, a* and b*).

DISCUSSION

This paper is, to our knowledge, the first to objectively quantify lifetime exposure to sun and to evaluate the relationship between this and ARM.

Our study shows that facial wrinkle length is positively related to late ARM prevalence, so lifetime exposure to sunlight and late ARM are considered to be positively related. Although it is conventionally held that hyperpigmentation and late ARM are related to lifetime exposure to sunlight, our results, in fact, show the opposite—that is, people with late ARM have fewer facial hyperpigmentation spots. This is difficult to explain; however, a relationship may exist between individual characteristics—that is, a skin that is strongly resistant to tanning and ARM.

Skin wrinkling has been suspected to be strongly associated with lifetime exposure to sunlight.[22–24] Skin wrinkling is related to an increase in collagen degradation in the extracellular matrix and to a decrease in its synthesis.[25] UV irradiation affects wrinkle formation through a cumulative process, so it is logical that facial wrinkling may be an indicator of lifetime exposure to sunlight.[18 19 22]

A significantly smaller area of hyperpigmented spots was, however, found in late ARM, despite the fact that our previous report concluded that hyperpigmentation was also increased by lifetime exposure to sun.[18] It may be that sunlight/UV irradiation induces changes in skin pigmentation, but the biological pathway differs from that of wrinkle formation. Skin darkening in response to UV irradiation occurs via two distinct pathways: immediate

pigment darkening and delayed tanning. Delayed tanning involves melanogenesis and is stimulated by DNA photodamage or its repair.[26] Melanin synthesis is therefore thought to be a direct response to DNA damage, and melanogenesis is viewed as a biomarker of DNA repair capacity. People with less pigmentation may be more vulnerable to DNA damage caused by exposure to sunlight. Type 1 Fitzpatrick skin types, those with fair-coloured skin and poor tanning ability, are known to be highly susceptible to skin cancer.[27 28] We hypothesise that genetic factors related to skin pigmentation are also related to ARM progression in Japanese men in Kagoshima.

With regard to the retina, melanin can act biochemically as an antioxidant in retinal pigment epithelial cells, lessening the harmful effects of UV-induced oxygen free radicals.[26] Ocular melanin is thought to be able to physically protect the retina and choroid of pigmented eyes against light-induced cell toxicity through UV absorption. The protection against UV damage afforded by melanin, presumably through a biochemical mechanism, may explain why ARM is more common in lighter-skinned populations.[29]

This study has certain limitations. There may be concern that exposure of facial skin to sunlight does not exactly reflect exposure of the ocular fundus to sunlight. All participants were male farmers with similar lifestyles in this rural area—for example, sunglasses are rarely used, diets are similar and individual differences would not be large. Although the sample was not large, two well-known risk factors for ARM, aging and smoking, were found to be significant for ARM. Because greater facial wrinkling is also a significant risk factor for late ARM, the sample size was sufficient for a preliminary identification of an additional risk factor for this condition. A potential subject selection bias exists in the study. Subjects with greater exposure to sunlight tend to have severe cataracts and may have been excluded because fundus photographs could not be taken. Of particular note is that age was not matched equally in the ARM groups compared with controls. Although age was applied as a covariant and the multiple variant analysis was performed in an age-adjusted way, the present results should be interpreted with care. It is not possible to say that the present method is perfectly objective. In fact, the definition of wrinkle that we used is subject to interpretation. Although the algorithm thresholds for wrinkle detection are subject to interpretation, the use of computer image analysis to objectively quantify wrinkle length and areas of hyperpigmentation eliminates the potential for bias and error associated with standard visual grading.

There are various other factors that can affect skin condition. Wrinkle length and/or skin pigmentation does not indicate the risk of ARM in every individual clinically. The value of the present method lies rather in its usefulness to study the pathogenesis of ARM.

In conclusion, this study suggests that lifetime exposure to sunlight is associated with ARM in Japanese men living in Kagoshima, Japan. Individual response to acute/chronic exposure to sun may be important in the progression of ARM. Because the objective methods used to measure skin wrinkling and hyperpigmentation such as markers of lifetime exposure to sunlight are standardised across all subjects in the study, and are cost-effective, reproducible and non-invasive, a large-scale follow-up study on different populations would be warranted to better elucidate the role of sun exposure in the progression of ARM and would be useful in the design and development of effective prophylactic treatments.

Funding: This work was supported in part by a grant from the Research Committee on Chorioretinal Degeneration and Optic Atrophy, Ministry of Health, Labor, and Welfare of Japan and by a Grant-in-Aid for Scientific Research from the Japanese Ministry of Education, Science, and Culture No 17390469.

Competing interests: None.

Ethics approval: Ethics approval was obtained.

Patient consent: Patient consent has been obtained for publication of fig 1.

REFERENCES

1. **Meyers SM.** A twin study on age-related macular degeneration. *Trans Am Ophthalmol Soc* 1994;**92**:775–843.
2. **Heiba IM,** Elston RC, Klein BE, *et al*. Sibling correlations and segregation analysis of age-related maculopathy: the Beaver Dam Eye Study. *Genet Epidemiol* 1994;**11**:51–67.
3. **Despriet DD,** Klaver CC, Witteman JC, *et al*. Complement factor H polymorphism, complement activators, and risk of age-related macular degeneration. *JAMA* 2006 19;**296**:301–9.
4. **Eye Disease Case-Control Study Group.** Risk factors for neovascular age-related macular degeneration. *Arch Ophthalmol* 1992;**110**:1701–8.
5. **Klein R,** Klein BE, Tomany SC, *et al*. Ten-year incidence of age-related maculopathy and smoking and drinking: the Beaver Dam Eye Study. *Am J Epidemiol* 2002;**156**:589–98.
6. **Seddon JM,** Cote J, Davis N, *et al*. Progression of age-related macular degeneration: association with body mass index, waist circumference, and waist-hip ratio. *Arch Ophthalmol* 2003;**121**:785–92.
7. **Khan JC,** Thurlby DA, Shahid H, *et al*. Genetic Factors in AMD Study. Smoking and age related macular degeneration: the number of pack years of cigarette smoking is a major determinant of risk for both geographic atrophy and choroidal neovascularisation. *Br J Ophthalmol* 2006;**90**:75–80.
8. **Taylor HR,** Munoz B, West S, *et al*. Visible light and risk of age-related macular degeneration. *Trans Am Ophthalmol Soc* 1990;**88**:163–73.
9. **Taylor HR,** West S, Munoz B, *et al*. The long-term effects of visible light on the eye. *Arch Ophthalmol* 1992;**110**:99–104.
10. **Cruickshanks KJ,** Klein R, Klein BE. Sunlight and age-related macular degeneration. The Beaver Dam Eye Study. *Arch Ophthalmol* 1993;**111**:514–18.
11. **Tomany SC,** Klein R, Klein BE. The relationship between iris color, hair color, and skin sun sensitivity and the 10-year incidence of age-related maculopathy: the Beaver Dam Eye Study. *Ophthalmology* 2003;**110**:1526–33.
12. **Darzins P,** Mitchell P, Heller RF. Sun exposure and age-related macular degeneration. An Australian case-control study. *Ophthalmology* 1997;**104**:770–6.
13. **Mitchell P,** Smith W, Wang JJ. Iris color, skin sun sensitivity, and age-related maculopathy. The Blue Mountains Eye Study. *Ophthalmology* 1998;**105**:1359–63.
14. **West SK,** Rosenthal FS, Bressler NM, *et al*. Exposure to sunlight and other risk factors for age-related macular degeneration. *Arch Ophthalmol* 1989;**107**:875–9.
15. **Hirvela H,** Luukinen H, Laara E, *et al*. Risk factors of age-related maculopathy in a population 70 years of age or older. *Ophthalmology* 1996;**103**:871–7.
16. **Delcourt C,** Carriere I, Ponton-Sanchez A, *et al*. Light exposure and the risk of age-related macular degeneration: the Pathologies Oculaires Liees a l'Age (POLA) study. *Arch Ophthalmol* 2001;**119**:1463–8.
17. **Khan JC,** Shahid H, Thurlby DA, *et al*. Genetic Factors in AMD Study. Age related macular degeneration and sun exposure, iris colour, and skin sensitivity to sunlight. *Br J Ophthalmol* 2006;**90**:29–32.
18. **Hillebrand GG,** Miyamoto K, Schnell B, *et al*. Quantitative evaluation of skin condition in an epidemiological survey of females living in northern versus southern Japan. *J Dermatol Sci* 2001;**27**(Suppl 1):S42–52.
19. **Akiba S,** Shinkura R, Miyamoto K, *et al*. Influence of chronic UV exposure and lifestyle on facial skin photo-aging: results from a pilot study. *J Epidemiol* 1999;**9**:S136–42.
20. **Bird AC,** Bressler NM, Bressler SB, *et al*. An international classification and grading system for age-related maculopathy and age-related macular degeneration. International ARM Epidemiological Study Group. *Surv Ophthalmol* 1995;**39**:367–74.
21. **Prignot J.** Quantification and chemical markers of tobacco-exposure. *Eur J Respir Dis* 1987;**70**:1–7.
22. **Hillebrand GG,** Levine MJ, Miyamoto K. The age-dependent changes in skin condition in ethnic populations from around the world. In: Berardesca E, Leveque J-L, Maibach H (eds) *Ethnic skin and hair*. New York: Informa Healthcare USA, 2006:105.
23. **Miyamoto K,** Hillebrand GG. The Beauty Imaging System: for the objective evaluation of skin condition. *J Cosmetic Sci* 2002;**53**:62–5.
24. **Warren R,** Gartstein V, Kligman AM, *et al*. Age, sunlight, and facial skin: a histologic and quantitative study. *J Am Acad Dermatol* 1991;**25**:751–60.
25. **Fisher GJ,** Wang ZQ, Datta SC, *et al*. Pathophysiology of premature skin aging induced by ultraviolet light. *N Engl J Med* 1997;**337**:1419–28.
26. **Agar N,** Young AR. Melanogenesis: a photoprotective response to DNA damage? *Mutat Res* 2005;**571**:121–32.
27. **Fitzpatrick TB.** The validity and practicality of sun-reactive skin types I through VI. *Arch Dermatol* 1988;124:869–71.
28. **Nilsson SE,** Sundelin SP, Wihlmark U, *et al*. Aging of cultured retinal pigment epithelial cells: oxidative reactions, lipofuscin formation and blue light damage. *Doc Ophthalmol* 2003;**106**:13–16.
29. **Kokkinou D,** Kasper HU, Schwarz T, *et al*. Zinc uptake and storage: the role of fundus pigmentation. *Graefes Arch Clin Exp Ophthalmol* 2005;**243**:1050–5.

Laboratory Investigation (2009) 89, 278–289

10

Intraocular expression and release of high-mobility group box 1 protein in retinal detachment

Noboru Arimura[1,2], Yuya Ki-i[1,2], Teruto Hashiguchi[2], Ko-ichi Kawahara[2], Kamal K Biswas[2], Makoto Nakamura[3], Yasushi Sonoda[1], Keita Yamakiri[1], Akiko Okubo[1], Taiji Sakamoto[1] and Ikuro Maruyama[2]

High-mobility group box 1 (HMGB1) protein is a multifunctional protein, which is mainly present in the nucleus and is released extracellularly by dying cells and/or activated immune cells. Although extracellular HMGB1 is thought to be a typical danger signal of tissue damage and is implicated in diverse diseases, its relevance to ocular diseases is mostly unknown. To determine whether HMGB1 contributes to the pathogenesis of retinal detachment (RD), which involves photoreceptor degeneration, we investigated the expression and release of HMGB1 both in a retinal cell death induced by excessive oxidative stress *in vitro* and in a rat model of RD-induced photoreceptor degeneration *in vivo*. In addition, we assessed the vitreous concentrations of HMGB1 and monocyte chemoattractant protein 1 (MCP-1) in human eyes with RD. We also explored the chemotactic activity of recombinant HMGB1 in a human retinal pigment epithelial (RPE) cell line. The results show that the nuclear HMGB1 in the retinal cell is augmented by death stress and upregulation appears to be required for cell survival, whereas extracellular release of HMGB1 is evident not only in retinal cell death *in vitro* but also in the rat model of RD *in vivo*. Furthermore, the vitreous level of HMGB1 is significantly increased and is correlated with that of MCP-1 in human eyes with RD. Recombinant HMGB1 induced RPE cell migration through an extracellular signal-regulated kinase-dependent mechanism *in vitro*. Our findings suggest that HMGB1 is a crucial nuclear protein and is released as a danger signal of retinal tissue damage. Extracellular HMGB1 might be an important mediator in RD, potentially acting as a chemotactic factor for RPE cell migration that would lead to an ocular pathological wound-healing response.

Laboratory Investigation (2009) **89,** 278–289; doi:10.1038/labinvest.2008.165; published online 12 January 2009

KEYWORDS: danger signal; high-mobility group box 1 protein; photoreceptor degeneration; retinal detachment; tissue damage; wound healing

Cell death is the predominant event of degenerative tissue damage and can be a trigger that activates the immune system and repair program. Recently, there has been much interest in the pivotal role of endogenous danger signals released during cell death.[1] High-mobility group box 1 (HMGB1) protein is a prototypic innate danger signal, and appears to be crucial in this context because extracellular HMGB1[2] can modulate inflammation, proliferation, and remodeling, which are involved in the wound-healing process.[3]

HMGB1 was originally described as an abundant and ubiquitous nuclear DNA-binding protein that had multiple functions dependent on its cellular location.[2,4] In the nucleus, HMGB1 binds to DNA and is critical for proper transcriptional regulation. It is also called amphoterin and accelerates cellular motility on the cell surface.[5] HMGB1 is reported to be passively released into the extracellular milieu by necrotic cells, but not by apoptotic cells,[6] or is exported actively by monocytes/macrophages[7] and neural cells[8] upon receiving appropriate stimuli. In damaged tissue, extracellular HMGB1 acts as a necrotic signal, which alerts the surrounding cells and the immune system.[2] Although extracellular HMGB1 can contribute to normal tissue development and repair, it is also implicated in the pathogenesis of several diseases (including lethal endotoxemia,[7] disseminated intravascular coagulation,[9] ischemic brain,[10] tumor,[11] atherosclerosis,[12] rheumatoid arthritis,[13] and periodontitis[14]).

[1]Department of Ophthalmology, Kagoshima University Graduate School of Medical and Dental Sciences, Kagoshima, Japan; [2]Department of Laboratory and Vascular Medicine, Kagoshima University Graduate School of Medical and Dental Sciences, Kagoshima, Japan and [3]Division of Ophthalmology, Department of Surgery, Kobe University Graduate School of Medicine, Kobe, Japan
Correspondence: Professor T Sakamoto, MD, PhD, Department of Ophthalmology, Kagoshima University Graduate School of Medical and Dental Sciences, 8-35-1, Sakuragaoka, Kagoshima 890-8520, Japan.
E-mail: tsakamot@m3.kufm.kagoshima-u.ac.jp

Received 25 August 2008; revised 9 October 2008; accepted 13 October 2008

Retinal detachment (RD), the physical separation of photoreceptors from the underlying retinal pigment epithelium (RPE), is one of the main causes of visual loss. Photoreceptor degeneration due to RD is thought to be executed by apoptosis[15,16] and necrosis,[17] which usually occur after tissue damage. Although retinal cell death and the following reactive responses must occur in almost all forms of retinal disease including RD,[18] data regarding the relationship among cell death, danger, and responses in the eye, have been very limited, especially in terms of danger signals. We previously reported that HMGB1 was significantly elevated in inflamed eyes with endophthalmitis, and suggested a possible link between HMGB1 and ocular inflammatory diseases.[19] On the other hand, considering the properties of HMGB1, we hypothesized that HMGB1 might have some roles in photoreceptor degeneration and subsequent damage-associated reactions in RD.

To investigate whether HMGB1 is involved in the pathogenesis of RD, we first examined the expression and release of HMGB1 both in a retinal cell death *in vitro* and in a rat model of RD-induced photoreceptor degeneration *in vivo*. To focus on human RD, we assessed the intravitreous concentrations of HMGB1 in human eyes affected by RD. Monocyte chemoattractant protein 1 (MCP-1), which was recently documented to be a potential proapoptotic mediator in RD,[20] was also measured in the same vitreous samples. We further analyzed the effects of recombinant HMGB1 (rHMGB1) on chemotactic activity in a RPE cell line *in vitro*. Our findings suggest that extracellular HMGB1 is evident in eyes with RD as a danger signal, potentially acting as a chemotactic factor for RPE cell migration that would lead to ocular pathological wound healing.

MATERIALS AND METHODS

Reagents

Full-length, LPS-free rat rHMGB1 protein, which is 99% identical to human HMGB1 and is fully functional on cells of mammalian origin,[21] was purchased from HMGBiotech (Milan, Italy). Human recombinant MCP-1 (rMCP-1) was purchased from Peprotec (Rocky Hill, NJ). Rabbit polyclonal antibody against HMGB1 was provided by Shino-Test Corporation (Kanagawa, Japan). Antibodies against phospho- and total extracellular signal-regulated kinase (ERK)-1/2 were obtained from Cell Signaling Technology (Beverly, MA). U0126 was obtained from Calbiochem (La Jolla, CA).

Human Vitreous Samples

This study was approved by our institutional ethical committee (Kagoshima University Hospital), and was performed in accordance with the Declaration of Helsinki. All surgeries were performed at Kagoshima University Hospital. All patients gave informed consent before treatment. The clinical histories of all patients were obtained from their medical records. Undiluted vitreous fluid samples (0.5–0.7 ml) were obtained by pars plana vitrectomy. Vitreous humor was collected in sterile tubes, placed immediately on ice, centrifuged to remove cells and debris, and stored at −80°C until analysis.

Animals

All animal experiments were performed in accordance with the Association for Research in Vision and Ophthalmology Statement for the Use of Animals in Ophthalmic and Visual Research and the approval of our institutional animal care committee (Kagoshima University). Adult male Brown Norway rats (250–300 g; KBT Oriental, Saga, Japan) were housed in covered cages and kept at constant temperature and relative humidity with a regular 12-h light–dark schedule. Food and water were available *ad libitum*.

Surgical Induction of RD

Rat experimental RD was induced as described previously.[22] Briefly, the rats were anesthetized with an intramuscular injection of ketamine and xylazine, and their pupils were dilated with topical 1% tropicamide and 2.5% phenylephrine hydrochloride. The retinas were detached using a subretinal injection of 1% sodium hyaluronate (Opegan; Santen, Osaka, Japan) with an anterior chamber puncture to reduce intraocular pressure. Sodium hyaluronate (0.05 ml) was slowly injected through the sclera into the subretinal space to enlarge the RDs. These procedures were performed only in the right eye, with the left eye serving as a control. Eyes with lens injury, vitreous hemorrhage, infection, and spontaneous reattachment were excluded from the following analysis. The rats were killed at 3, 7, and 14 days after treatment, with six animals per each time point.

Cell Culture

The rat immortalized retinal precursor cell line R28, a kind gift from Dr GM Siegel (The State University of New York, Buffalo), was cultured in Dulbecco's modified Eagle's medium (DMEM) high glucose supplemented with 10% fetal bovine serum (FBS), 10 mM non-essential amino acids, and 10 μg/ml gentamicin as described previously.[23] The human immortalized RPE cell line ARPE-19, obtained from American Type Culture Collection (Manassas, VA), was grown in DMEM/F12 supplemented with 10% FBS, 2% penicillin–streptomycin, and 1% fungizone (all products were obtained from Invitrogen-Gibco, Rockville, MD). Cells were incubated at 37°C in a 5% CO_2 incubator and subcultured with 0.05% trypsin-EDTA. Subconfluent cultures were trypsinized and seeded for the following experiments. ARPE-19 cells were obtained at passage 21 and used at passages 24–30. Increased passage did not alter the following experimental results up to this passage number.

Cell Viability Assay

Cell viability was analyzed by mitochondrial respiratory activity measured using MTT (3-(4,5-dimethylthiazol-2yl)-2,5-diphenol tetrazolium bromide) assay (Wako Chemicals,

Osaka, Japan), as described previously.[24] Briefly, 2×10^5 R28 cells were cultured in 24-well plates (500 μl medium per well) with or without hydrogen peroxide (1 mM; Merck, Darmstadt, Germany) for 24 h. Then the cells were incubated with MTT (0.5 mg/ml; final concentration) for 3 h. Formazan product was solubilized by the addition of dimethyl sulfoxide for 16 h. Dehydrogenase activity was expressed as absorbance at a test wavelength of 570 nm and at a reference wavelength of 630 nm. Assays were performed in triplicate and repeated three times in independent experiments.

Immunofluorescence for HMGB1 and TUNEL

Indirect immunofluorescence was carried out as described previously,[19,25] with some modifications. The eyes were harvested and fixed in 4% paraformaldehyde at 4°C overnight. The anterior segment and the lens were removed, and the remaining eye cup was cryoprotected with 10–30% sucrose in phosphate-buffered saline. The eye cups were then frozen in an optimal cutting temperature compound (Sakura Finetech, Tokyo, Japan). Sections were cut at 8 μm with a cryostat (Leica Microsystems, Wetzler, Germany). After being incubated with blocking buffer containing 10% goat serum, 1% bovine serum albumin (BSA), and 0.05% Tween-20 for 1 h, the slides were incubated with rabbit polyclonal anti-HMGB1 antibody (1 μg/ml). After overnight incubation, sections were washed and probed with Alexa-Fluor 594-conjugated goat anti-rabbit IgG F(ab')2 fragment (Molecular Probes, Carlsbad, CA) for 1 h. In some experiments, TUNEL co-staining was also performed according to the manufacturer's protocol (ApopTag Fluorescein *In situ* Apoptosis Detection kit; Chemicon, Temecula, CA) as previously described.[22] Slides were counterstained with DAPI, mounted with Shandon PermaFlour (Thermo Scientific, Waltham, MA), and viewed with a Zeiss fluorescence microscope. Images were captured using the same exposure time for each comparative section. To examine the specificity of immunostaining, the primary antibody was replaced with normal rabbit IgG (1 μg/ml). Control slides were invariably negative under the same setting (data not shown). For all experiments, at least three sections from each eye were evaluated. To demonstrate the expression patterns of HMGB1 in retinal cells under oxidative stress *in vitro*, R28 cells (2×10^5 cells/500 μl medium per well) were seeded on four-well glass coverslips and challenged with or without hydrogen peroxide (1 mM) for 1 h. Slides were fixed in 4% paraformaldehyde for 1 h, permeabilized with Triton X-100, and then examined by the same methods as described above.

ELISAs

HMGB1 and MCP-1 were quantified in each human vitreous sample using commercial ELISAs; HMGB1 ELISA kit (Shino-Test Corporation) and Human CCL2/MCP-1 Immunoassay (R&D Systems, Minneapolis, MN), according to the manufacturers' protocols. The detection limits of these kits were 0.2 ng/ml for HMGB1 and 5.0 pg/ml for MCP-1. Concentrations below the limits were taken as zero in subsequent analyses. Each sample was run in duplicate and compared with a standard curve. All samples were assessed in a masked manner. The mean concentration was determined per sample. For *in vitro* study, HMGB1 levels in culture supernatants were measured by the same ELISA.

Migration Assay

Cell migration was assayed using a modified Boyden chamber assay as previously described.[26] In brief, 5×10^4 ARPE-19 cells resuspended in 200 μl control medium (1% FBS-DMEM/F12) were seeded onto the upper compartment of the BD Falcon® culture inserts (BD Bioscience, San Jose, CA) with an 8-μm diameter pore size membrane in a 24-well companion plate. The lower chamber was filled with control medium (negative control) and those containing 50, 100, or 200 ng/ml rHMGB1. Because MCP-1 was reported to display a potent chemotactic activity on RPE cells,[27] a control medium containing 10 ng/ml rMCP-1 was used as a positive control. After 8-h incubation, cells remaining on the upper surface of the filters were removed mechanically, and those that had migrated to the lower surface were fixed with methanol, stained with Diff-Quick (Dade-Behring, Deerfield, IL), and counted in five randomly selected high-power fields ($\times$ 100) per insert. Migration index (% of control) was calculated by dividing the number of migrating cells in the presence of chemoattractants by the cells that migrated in response to the negative control. To inhibit ERK-1/2 activity, the cells were pretreated with 1, 5, or 10 μM U0126, or vehicle (0.1% dimethyl sulfoxide) for 30 min, prior to the addition of rHMGB1. U0126 is an inhibitor of active and inactive MEK-1/2, the MAPK kinase that activates ERK-1/2. These concentrations of U0126 and dimethyl sulfoxide had no effect on ARPE-19 cell viability determined by MTT assay in our study (data not shown) and in a previous report.[28] Assays were performed in triplicate and repeated three times in independent experiments.

Immunoblotting

ARPE-19 cells (5×10^5) were subcultured on 6-cm tissue culture dishes. Then, the cells were serum starved overnight in DMEM/F12 and stimulated with 100 ng/ml rHMGB1 for the indicated times. Activation of ERK-1/2 was analyzed as described previously.[24] In brief, after treatment, whole cells were lysed with SDS sample buffer and an equal volume of protein extracts was loaded onto 12% SDS-polyacrylamide gels and then transferred onto a nitrocellulose membrane. The membrane was blocked by incubation with 5% non-fat dry milk plus 1% BSA in TBST (0.02% Tween-20 in Tris-buffered saline, pH 7.4) for 1 h at room temperature. The membrane was then incubated with the antibody against phospho-ERK-1/2 (diluted 1/1000) at 4°C overnight. The blots were subsequently probed with secondary anti-rabbit antibodies conjugated to horseradish peroxidase (diluted 1/3000 in TBST), and images were developed using the en-

hanced chemiluminescence system (GE Healthcare). The membrane was stripped and reprobed with an antibody against total ERK-1/2 (diluted 1/1000).

Statistical Analysis

The vitreous HMGB1 and MCP-1 concentrations in each group were compared using the Mann–Whitney *U*-test. The correlation between HMGB1 and MCP-1 in RD samples was analyzed using a simple linear regression analysis and Spearman's rank correlation coefficient. All *in vitro* data are presented as mean ± s.d. and the significance of differences between groups was determined by Student's *t*-test. *P*-value less than 0.05 was considered significant.

RESULTS

HMGB1 is Present in Cultured Retinal Cell and Released Extracellularly by Oxidative Stress-Induced Cell Death

We first evaluated the expression patterns and cellular distribution of HMGB1 in an R28 retinal cell line with or without oxidative stress, a known cause of neurodegeneration.[29] Excessive reactive oxygen species can lead to the destruction of cellular components and ultimately induce cell death through apoptosis or necrosis. To induce oxidative stress, we used a toxic dose (1 mM) of hydrogen peroxide, which was reported to stimulate monocytes/macrophages to release HMGB1 actively and passively.[30] As shown in Figure 1a, HMGB1 immunoreactivity was stably present in the nucleus of unstimulated R28 cells, and relatively weak staining was observed in the cytoplasm. By contrast, 1 h after exposure to 1 mM hydrogen peroxide, some cells seemed to present rather high levels of HMGB1 in their nucleus as well as their cytoplasm compared with those under an unstimulated condition. However, in the other cells, the nuclear HMGB1 was diminished or appeared to be released into the cytoplasm. These results indicate that the nuclear HMGB1 could be varied by death stress and be released into the cytoplasm according to the degree of stress. Hydrogen peroxide (1 mM) treatment for 24 h, in which about 90% of the cells lost their viability (Figure 1b), induced a massive release of HMGB1 from the cells to the cell supernatants (Figure 1c). Taken together, these findings suggested that HMGB1 could relocate from the nucleus to the cytoplasm for eventual release in dying retinal cells, and that the extracellular release of HMGB1 in the eye might be increased dependent on the extent of retinal cell death.

HMGB1 is Abundantly Expressed in Rat Retina and Released after RD

As the above findings indicated that HMGB1 was of relevance to retinal cell death, we investigated whether HMGB1 was maintained in the rat retina and how HMGB1 would vary after RD. As it was reported that HMGB1 in rat photoreceptors had a light-sensitive circadian rhythmic expression,[25] we performed all animal studies on a regular time schedule, and all eyes were set to be almost equally exposed to light. As shown in Figure 2, HMGB1 immunoreactivity was well represented in sections of the normal control rat retina and, as expected, colocalized with DAPI-positive nuclei (Figure 2a, d and g). HMGB1 staining in the normal rat retina was prominent in the nuclei of ganglion cell layer, inner nuclear layer, outer nuclear layer, and RPE, and was also apparent in the photoreceptor inner segments. In particular, HMGB1 was localized in photoreceptor at the nuclear periphery, and HMGB1 levels were higher in the inner nuclear layer than the outer nuclear layer as opposed to DAPI staining, which preferred to bind to heterochromatic DNA. This was consistent with the previous report[25] that HMGB1 was preferentially colocalized with euchromatin, which was often under active transcription and was stained less by DAPI. Interestingly, HMGB1 appeared to be robustly upregulated in both the photoreceptors and the other retinal cells at day 3 after RD inductions, and DAPI staining was inversely downregulated at the same time (Figure 2b, e and h). As previous reports demonstrated that dramatic alterations of retinal gene expression occurred after RD,[31] this high level of HMGB1 expression might be related to the active gene transcription. HMGB1 in the nucleus might be stress responsive and necessary for proper transcription after RD tissue damage. Afterwards, the nuclear HMGB1 expression in the photoreceptors seemed to subside at day 7, while still clearly remained in the inner segments (Figure 2c, f and i), gradually decreasing along with the thinning of the outer nuclear layer due to photoreceptor degeneration by day 14 (data not shown).

Although HMGB1 expression was increased in the photoreceptors of the detached retina at day 3, it was not homogeneous, but was rather heterogeneous. To clarify the relationship between the upregulation of HMGB1 and photoreceptor cell death, especially with DNA damage, the RD retina at day 3 was co-stained with TUNEL, which could detect apoptotic and potentially necrotic cell death by labeling the damaged DNA (Figure 3a–c). Previous studies indicated that HMGB1 could not be released from apoptotic cells[6] and the apoptotic photoreceptors were prominent in this RD model at day 3 after RD.[22] We also confirmed remarkable numbers of apoptotic photoreceptors in the detached retina at day 3 (Figure 3b), and found that the early faint TUNEL-positive nuclei had relatively low levels of HMGB1 and fragmented nuclei, which were brightly stained by TUNEL, had almost no apparent HMGB1 immunoreactivity (Figure 3c), suggesting that apoptotic dying cells might lose the expression of HMGB1 to maintain the proper gene transcription. It might be indispensable for the surviving photoreceptors to maintain and/or boost the nuclear HMGB1 in RD.

In the subretinal space of RD at day 7, HMGB1-positive and TUNEL-negative debris could be observed (Figure 3d, arrows), which might be released by necrotic photoreceptors and/or degradated inner segments, and spread diffusely into the vitreous cavity if a retinal break was present. It was also

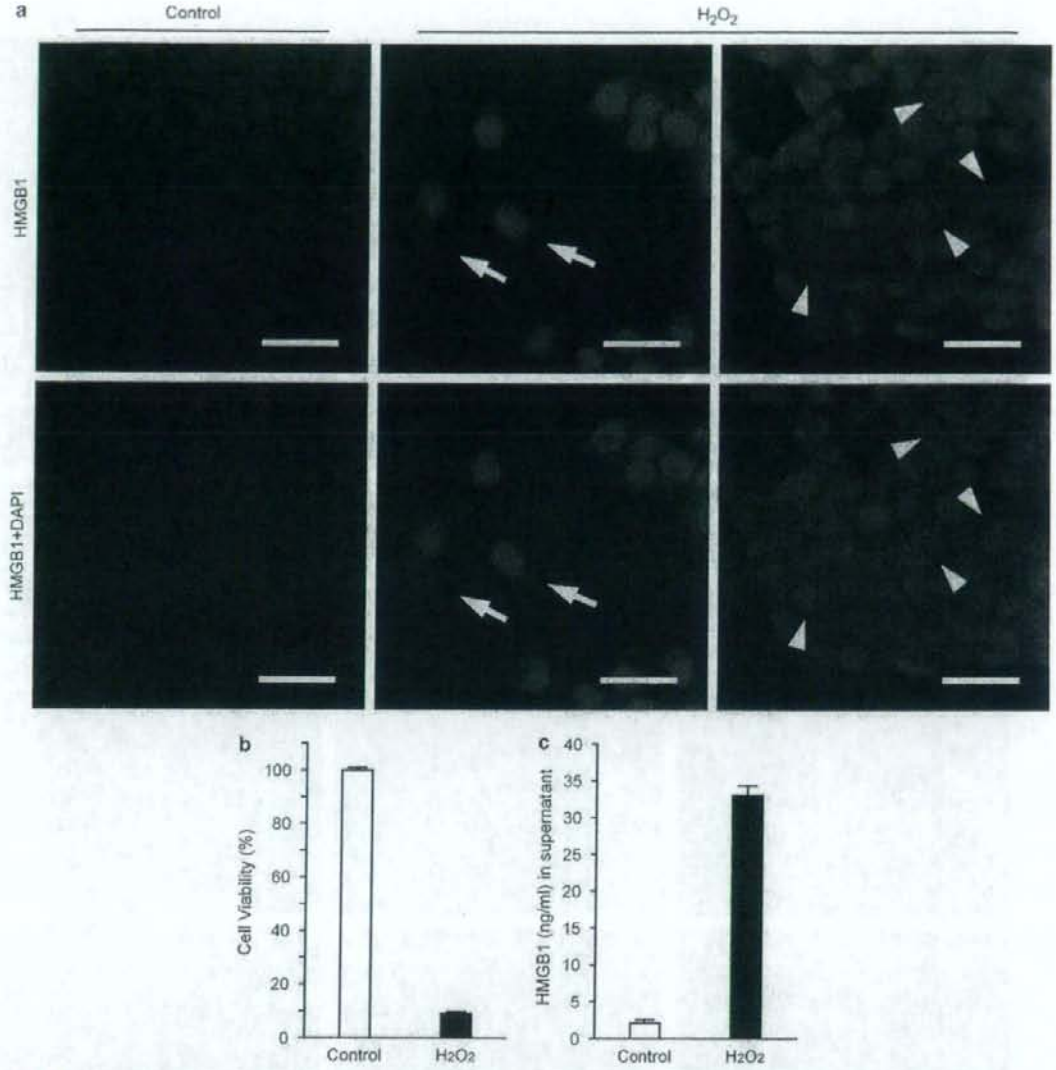

Figure 1 Release of HMGB1 from R28 retinal neuronal cells exposed to excessive oxidative stress. (**a**) Immunofluorescence was performed with anti-HMGB1 antibody (red) and DAPI (blue). HMGB1 is predominantly present in the nuclei of unstimulated R28 cells (left column). Some cells present robust upregulation of HMGB1 in the nuclei, as well as relocation into the cytoplasm (middle column; arrows) on 1 h exposure to a toxic dose of hydrogen peroxide (1 mM). In the other cells, the nuclear HMGB1 is found to be diminished or released into the cytoplasm (right column; arrowheads). Scale bars: 20 μm. (**b**) After 24 h exposure to 1 mM hydrogen peroxide, the cell viability analyzed by MTT assay is decreased to about 10% compared with the control. (**c**) Massive HMGB1 release into the culture supernatant was determined by ELISA after the same treatment as (**b**). The data represent the mean ± s.d. ($n = 3$). Similar results were obtained from three independent experiments.

Figure 2 Immunofluorescence analysis of HMGB1 in a rat model of RD. Representative photomicrographs of retinal sections labeled with anti-HMGB1 antibody (red; **a**–**c**) and DAPI (blue; **d**–**f**). Merged images (**g**–**i**) are also presented. The retinal sections were derived from the control eye (**a**, **d**, **g**), those at 3 days (day 3; **b**, **e**, **h**), or 7 days after RD (day 7; **c**, **f**, **i**). Arrows point to retinal pigment epithelium (**a**, **g**), and arrowheads indicate subretinal macrophages (**b**, **c**, **h**, **i**). Note that expression of HMGB1 is augmented especially in ONL at day 3 after RD, whereas the upregulation in ONL appears to be subside by day 7 ($n = 6$ for each time point). Scale bars: 50 μm. INL, inner nuclear layer; IS, inner segment; ONL, outer nuclear layer.

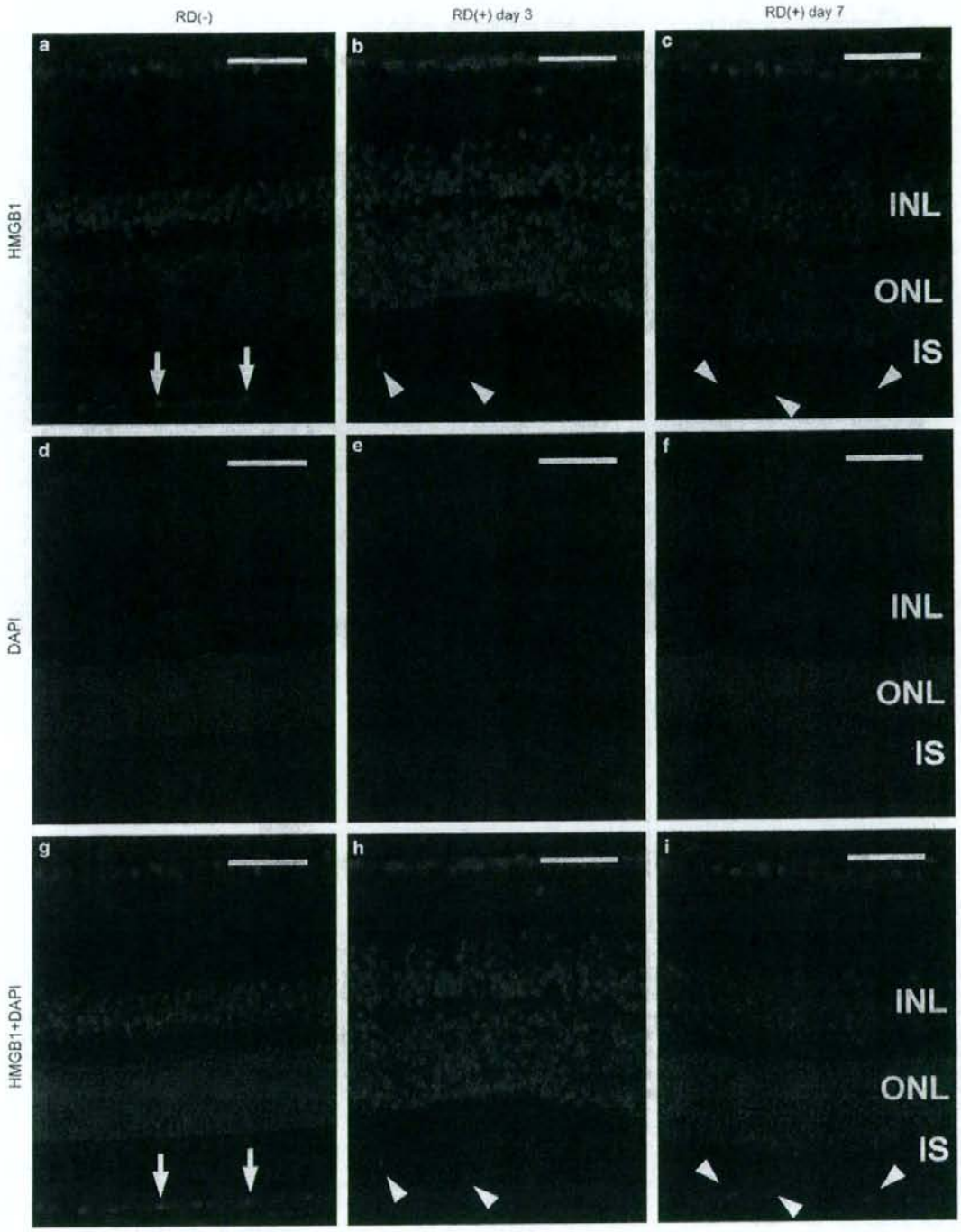
RD(-)
RD(+) day 3
RD(+) day 7
HMGB1
DAPI
HMGB1+DAPI
a
b
c
d
e
f
g
h
i
INL
ONL
IS
INL
ONL
IS
INL
ONL
IS

reported that macrophages migrated into the subretinal space of this RD model.[32] The migrating macrophages also had abundant HMGB1 expression (Figure 3d, arrowheads), and might have released HMGB1 actively in this space. In line with these data, a large amount of extracellular HMGB1 must be present at least in the subretinal space after RD.

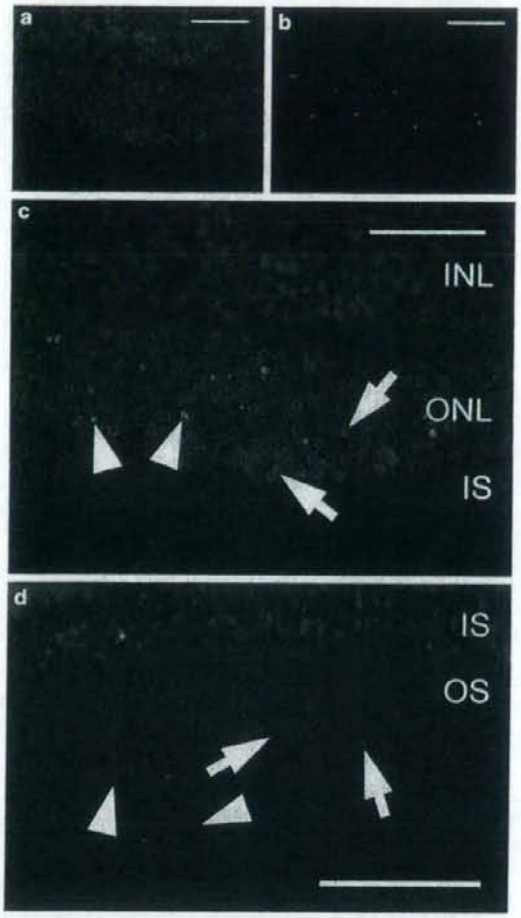

Figure 3 Expression of HMGB1 in DNA-damaged photoreceptors (**a**–**c**) and release of HMGB1 in the subretinal space (**d**). Representative photomicrographs of anti-HMGB1 antibody (red; **a**), TUNEL (green; **b**), and merged image (**c**) from rat retinal sections at 3 days after RD ($n=6$). The early faint TUNEL-positive nuclei (**c**; arrows) have relatively low levels of HMGB1 and the fragmented nuclei (**c**; arrowheads) have almost no apparent HMGB1 immunoreactivity. (**d**) Representative photomicrograph of a merged image of anti-HMGB1 (red), DAPI (blue), and TUNEL (green) obtained from rat retinal sections at 7 days after RD ($n=6$). HMGB1-positive and TUNEL-negative debris (**d**; arrows) and migrating macrophages with abundant HMGB1 expression (**d**; arrowheads) can be observed in the subretinal space. Scale bars: 50 μm. INL, inner nuclear layer; IS, inner segment; ONL, outer nuclear layer; OS, outer segment.

Vitreous HMGB1 and MCP-1 Levels in Patients with RD

The result obtained from the rat model of RD is the first evidence to our knowledge that HMGB1 is involved in RD-induced photoreceptor degeneration. Next, we tested whether extracellular HMGB1 could also be detected in human vitreous samples of RD. Samples were harvested from 35 eyes with RD, including rhegmatogenous RD, RD with macular hole, and atopic RD and 19 eyes with control diseases, including idiopathic epiretinal membrane and idiopathic macular hole (Table 1). The vitreous HMGB1 and MCP-1 levels were significantly higher in the eyes with RD than in those with control diseases (Figure 4). The median HMGB1 level was 1.4 ng/ml (range, 0–28.3) in the eyes with RD and 0.6 ng/ml (range, 0–1.3) in those with control diseases ($P<0.001$; Figure 4a). The median MCP-1 level was 1383.2 pg/ml (range, 39.8–5436.1) in the RD eyes and 404.4 pg/ml (range, 17.9–1168.9) in the control eyes ($P<0.0001$; Figure 4b). The vitreous concentration of HMGB1 was correlated significantly with that of MCP-1 in the 35 eyes with RD by a simple linear regression ($r=0.593$, $P<0.001$; Figure 4c) and by Spearman's rank correlation coefficient ($r=0.613$, $P<0.001$). On the other hand, there was no significant relationship between the vitreous concentrations of HMGB1 and MCP-1 in the 19 eyes of control patients (data not shown). Although there was no significant difference, the HMGB1 levels in the eyes with proliferative vitreoretinopathy (PVR), a condition of retinal fibrosis that follows severe long-standing RD, tended to be lower than those without PVR (Figure 4d). These findings showed that HMGB1 could be released not only in the subretinal space but also in the vitreous cavity after RD-induced photoreceptor degeneration, and that the HMGB1 release was coincident with vitreous MCP-1 expression.

Table 1 Characteristics of the patients

Characteristics	Retinal detachment ($n=35$)	Control diseases ($n=19$)
Age (years)	57.3 ± 16.3	68.2 ± 8.7
Female sex, no. (%)	19 (54)	10 (53)
Patients with PVR, no. (%)	6 (17)	—
Subgroups, no. (%)		
Rhegmatogenous retinal detachment	28 (80)	—
Retinal detachment with macular hole	5 (14)	—
Atopic retinal detachment	2 (6)	—
Idiopathic epiretinal membrane	—	7 (37)
Idiopathic macular hole	—	12 (63)

PVR, proliferative vitreoretinopathy.
Values are expressed as mean ± s.d. Dashes denote not applicable.

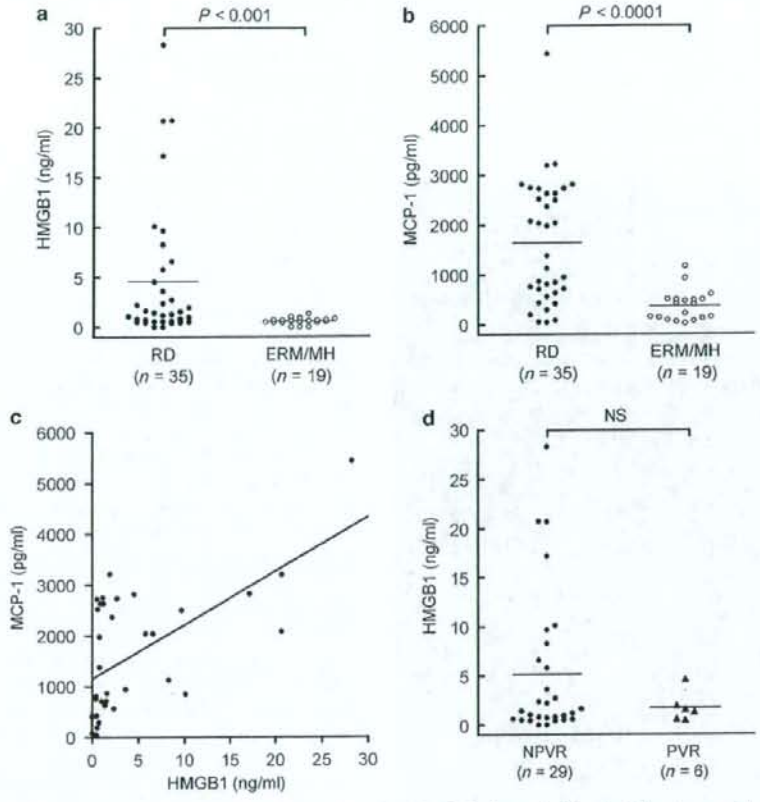

Figure 4 Vitreous levels of HMGB1 and MCP-1. The vitreous HMGB1 (**a**) and MCP-1 (**b**) levels are significantly higher in eyes with RD than in those with control diseases (idiopathic epiretinal membrane or idiopathic macular hole). Each bar indicates the average value. (**c**) Scatter plot for the correlation between vitreous levels of HMGB1 and MCP-1 in eyes with RD (simple linear regression, $r = 0.593$, $P < 0.001$; Spearman's rank correlation coefficient, $r = 0.613$, $P < 0.001$). (**d**) The HMGB1 levels in the eyes with PVR tend to be lower than those without PVR. ERM/MH, epiretinal membrane/macular hole; NPVR, no PVR; PVR, proliferative vitreoretinopathy.

RPE Cells Respond Chemotactically to Extracellular HMGB1 through an ERK-Dependent Mechanism

Previous reports have shown that extracellular HMGB1 is a chemoattractant for a variety of cell types.[21,33,34] We investigated whether HMGB1 is also a chemoattractant for RPE cells. Extracellular HMGB1 has been reported to engage multiple receptors, including the receptor for advanced glycation end products (RAGE) and Toll-like receptors 2 and 4.[2,4] In particular, RAGE has been thought to be a crucial receptor for HMGB1-induced cell migration through ERK activation.[33] The expression of RAGE at the RNA and protein level was identified in human RPE[35] and ARPE-19 cells[36,37] in previous studies. It was also shown that the expression of RAGE and HMGB1 was colocalized in the proliferative membrane from an eye with proliferative retinal disease.[38] We, therefore, performed a migration assay using modified Boyden chambers with various concentrations of rHMGB1. The representative photographs in Figure 5 show that rHMGB1 was capable of inducing a significant level of migration (Figure 5b) above that obtained with the control medium (Figure 5a). HMGB1 stimulated the migration of RPE cells in a concentration-dependent manner with a 2.7-fold maximal response at 100 ng/ml (Figure 5c). This maximal response to rHMGB1 was slightly stronger than that induced by rMCP-1 (10 ng/ml). Next, we investigated whether HMGB1 induced phosphorylation of ERK-1/2 in ARPE-19 cells; we stimulated cells with 100 ng/ml rHMGB1 for various time periods and used western blotting with an anti-phospho-ERK-1/2 antibody on whole-cell lysates (Figure 6a). Little phosphorylation of ERK-1/2 could be observed in unstimulated ARPE-19 (at 0 min), but a prominent increase was detected after 5 min of stimulation with rHMGB1. Figure 6a shows that phosphorylation of ERK-1/2 was augmented from 5 to 60 min after rHMGB1 stimulation in comparison

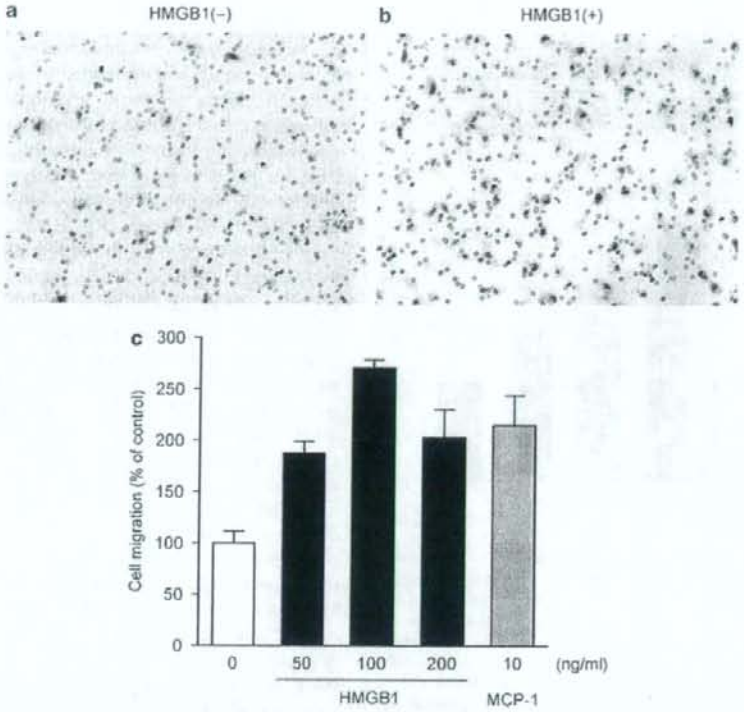

Figure 5 RPE cells migrate in response to HMGB1. Representative photographs of ARPE-19 cells stained with Diff-Quick after migration toward control medium (**a**) or 100 ng/ml HMGB1 (**b**). Original magnification: × 100. (**c**) HMGB1 stimulated ARPE-19 cell migration in a concentration-dependent manner with a 2.7-fold maximal response at 100 ng/ml. The data represent the mean ± s.d. ($n = 3$). All treatments increase the migratory response relative to the control ($P < 0.01$ in Student's *t*-test). Similar results were obtained from three independent experiments.

with unstimulated ARPE-19 (time 0). To demonstrate that the ERK signaling induced by HMGB1 was in fact linked to the migration of RPE cells, we next inhibited ERK-1/2 and assessed cell migration to HMGB1. Pretreatment of ARPE-19 with U0126 abrogated the migration toward rHMGB1 (Figure 6b). Thus, the ERK pathway appears to play an essential role in HMGB1-induced RPE cell migration.

DISCUSSION

Our findings suggest a possible role of HMGB1 in RD, as an essential nuclear protein and a principal danger signal for photoreceptor degeneration. Using an *in vitro* assay of retinal cell death induced by excessive oxidative stress, we found that HMGB1 was augmented in the nucleus by the stress and released into the extracellular space during cell death. On the basis of immunohistochemical analyses of a rat model of RD-induced photoreceptor degeneration, augmentation of HMGB1 in the nucleus is also observed *in vivo* and appears to be crucial for the proper transcription of photoreceptors after RD. Moreover, double labeling with TUNEL reveals defects of upregulation of the nuclear HMGB1 in the DNA-damaged photoreceptors, which are presumably programmed dying photoreceptors. Therefore, we propose that the nuclear HMGB1 in the retinal cells might be critical for retinal cell survival under death stresses both in the *in vivo* RD and *in vitro* retinal cell death. These results for ocular HMGB1 are compatible with previous reports that HMGB1 is a vital nuclear protein and has a protective role in the nucleus.[2,4]

In a previous animal study, Erickson *et al*[17] reported that a loss of photoreceptors in a cat model of RD occurred due to necrosis. During studies on RD, photoreceptor degeneration after RD had been thought to be mainly caused by apoptosis.[15,16] Hisatomi *et al*[32] demonstrated the presence of apoptotic debris in the subretinal space of rat RD. In the present study, considering our immunohistochemistry results from the same rat model of RD, so-called necrotic debris, which is HMGB1 positive and TUNEL negative, was found to be present. On the basis of the previous finding of the preferential release of HMGB1 from necrotic cells,[6] this suggests that necrosis might still be a fundamental type of photoreceptor cell death after RD.